ABSTRACT

INVESTIGATION OF OPEN-CAVITY RADIATORS

By

Min-Houng Hong

An open-cavity radiator, or a simplified model of recently developed "backfire" antennas, is investigated in this research. This antenna consists of a simple, open-ended circular cavity with a primary radiator placed at an appropriate location inside the cavity. The circuit property and the radiation characteristics of this radiator are studied.

The waveguide excitation theory is employed to find the field excited in the cavity. The aperture field is then determined by summing the propagating modes at the open end of the cavity. Subsequently, the radiation field is calculated based on the aperture field. The input resistance of the radiator is obtained from the total radiated power carried by the propagating modes and the input current of the primary radiator.

Various primary radiators such as a dipole, a dipole array, a transmission line and a circular loop are considered in this study.

An experimental study has been conducted in parallel with the theoretical analysis and a satisfactory agreement has been obtained between theory and experiment. This study may help clarify the mechanism of radiation of this new radiator and prove useful in its optimum design.

INVESTIGATION OF OPEN-CAVITY RADIATORS

By

Min-Houng Hong

A THESIS

Submitted to
Michigan State University
in partial fulfillment of the requirements
for the degree of

DOCTOR OF PHILOSOPHY

Department of Electrical Engineering and Systems Science

1970

To my parents

Mr. & Mrs. Chien-Chuan Hong

ACKNOWLEDGMENTS

The author wishes to express his sincere appreciation to his major professor, Dr. K. M. Chen, for his guidance and encouragement in the course of this research.

He also wishes to thank the committee member Dr. D. P. Nyquist for giving the valuable suggestions in this research, and to the other members, Dr. B. Ho and Dr. R. Hamelink, for reading the thesis.

Finally, the author owes a special thank to his wife, Ai-Hwei, for the encouragement and understanding that only a wife can give.

The research reported in this thesis was supported by Air Force Cambridge Research Laboratories under contract F 19628-70-C-0072.

TABLE OF CONTENTS

LIST OF FIGURES

LIST OF TABLES

CHAPTER 1

INTRODUCTION

Antennas employing the "backfire" principle conceived by Ehrespeck[1, 2] have been the subjects of extensive experimental studies. More recently, Ehrespeck[3] has developed a "short-backfire" antenna which consists of a simple open-ended circular cavity with a dipole exciter placed at an appropriate location inside the cavity and a small reflecting plate placed in the open end. A gain of 15 dB above isotropic, with side lobes of at least -20 dB and a back lobe lower than -30 dB was achieved with this configuration. In spite of its simple geometrical structure, this radiator has a comparable performance as a more sophisticated reflecter-type antenna. Although this antenna has been studied experimentally, very little theoretical work has been conducted.

Chen, Nyquist and Lin[4] have developed an approximate calculation of the radiation fields of a short "backfire" antenna based upon the assumption that the aperture field is distributed approximately cosinusoidally in both horizontal and vertical planes

as evidenced by a near-zone measurement. They conclude that a short "backfire" antenna is essentially a circular aperture antenna with the dipole functioning merely as an exciter for the aperture field. Zucker[5] has theoretically studied a long "backfire" antenna and has provided some useful information for design.

It is apparent that more extensive theoretical and experimental studies are needed to understand the basic operational principles of this radiator. It is also anticipated that if an adequate theory is developed, it will not only lead to an understanding of the basic principles of this antenna but perhaps may also lead to a better design for the backfire antenna or the development of a new class of open-cavity radiator type antennas. It is for these reasons that the present investigation was made.

The model of the radiator for this study is similar to that of a short "backfire" antenna except that the reflecting plate at the antenna aperture is ignored and the rim length of the antenna is increased. The reasons for adopting this model are for theoretical simplicity and for the experimental fact that a short "backfire" antenna radiates the same if the reflecting plate is removed while the antenna rim is increased.

In this investigation, both theoretical and experimental studies have been conducted to find the radiation and circuit properties of an open-cavity radiator excited by various primary exciters. For the primary exciters, a dipole, a dipole array, a

transmission line and a circular loop have been considered. The current distribution on the primary exciter is assumed. The waveguide excitation theory is employed to find the expansion coefficients of the normal modes excited in the cavity. The reflection coefficients of the normal modes at the open end of the cavity are calculated approximately. The aperture field is obtained by summing the propagating modes at the open end of the cavity; the radiation field is then calculated based on the aperture field. The input resistance is obtained by calculating the total radiated power carried by the propagating modes.

The effects of the cavity dimensions and the geometries and dimensions of the exciters on the radiation characteristics of the radiator are studied. Theory has been confirmed by experiment. The present investigation should prove useful in the understanding of the basic operational principles of a "backfire antenna" and its design.

CHAPTER 2

WAVEGUIDE EXCITATION THEORY AND THE RADIATION FIELDS OF THE OPEN-CAVITY RADIATORS

2.1 Geometry and Statement of the Problem

The geometry of an open-cavity radiator is as shown in Fig. 2.1. This antenna consists of a simple, open-ended circular cylinder with a primary radiator placed at an appropriate location inside the cylinder. The configuration of the primary radiator can be of various shapes. Various current sources $\vec{J}_a$ with the frequency ω are assumed to be on the primary radiator. The circular cylinder is assumed to be perfectly conducting with a radius of A and a length of $L = \ell_1 + \ell_2$. This cylinder is short-circuited by a perfect plane reflector at $z = -\ell_1$ and the other end is open at $z = \ell_2$. The center of the primary radiator is located at $z = 0$. Inside the cavity, or the open waveguide, cylindrical coordinates (r', ϕ', z) are adopted to express the waveguide fields. Outside the cavity, a new coordinate system is used to express the radiation fields.

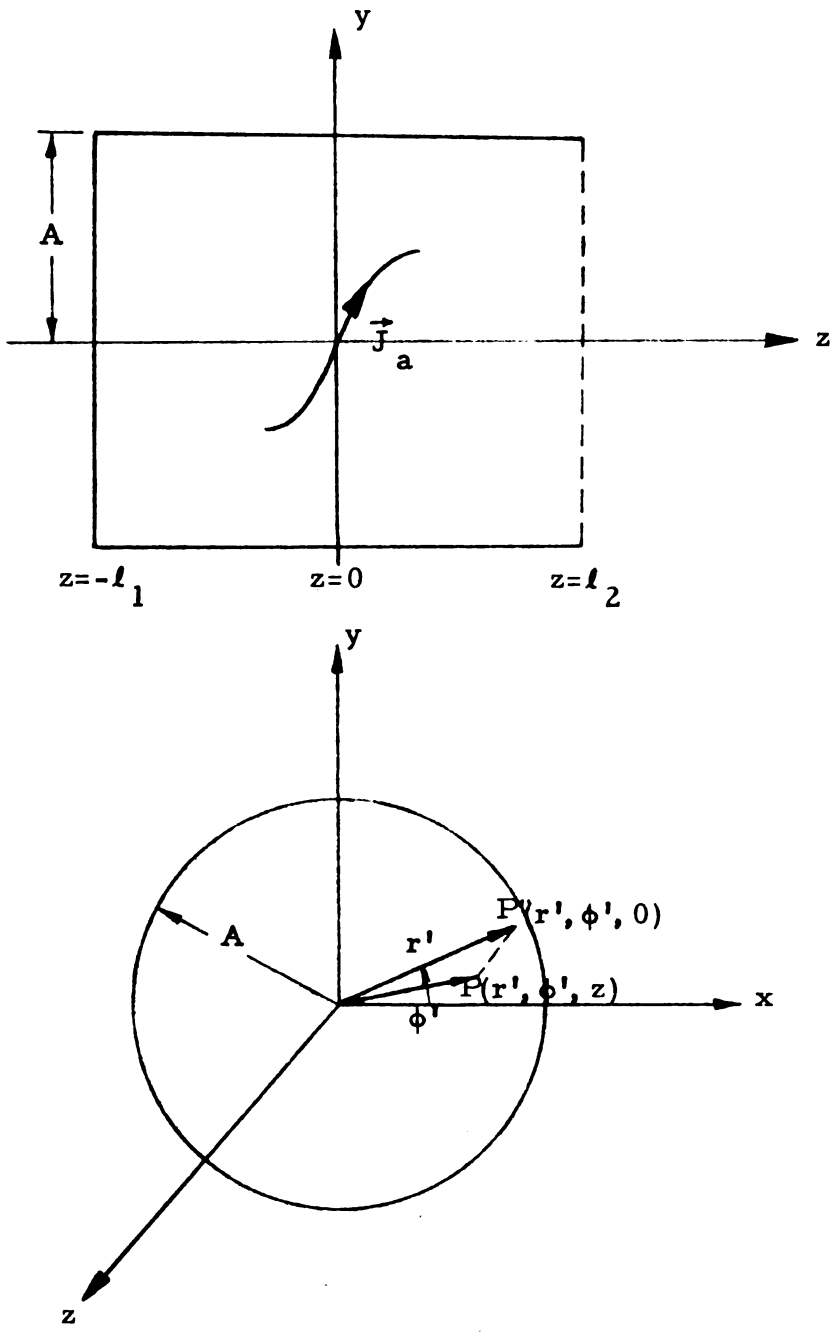

Fig. 2.1 Geometry of an open-cavity radiator

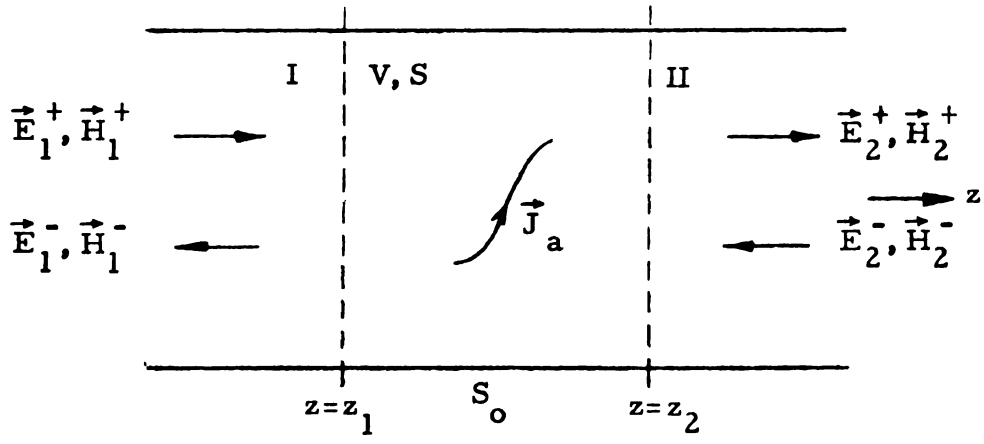

Region I: $z < z_1$

Region II: $z > z_2$

Source Region: $z_1 \leq z \leq z_2$

Fig. 2.2 Geometry and fields of a waveguide excited by source $\vec{J}_a$

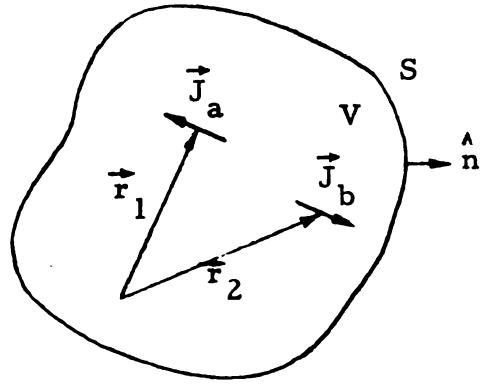

Fig. 2.3 Illustration for Lorentz Lemma

2.2 Waveguide Excitation Theory

In a circular cylindrical waveguide with a radius A which is relatively large compared with the wavelength, several waveguide modes can propagate along the waveguide. With a known current source located in the waveguide, the EM field can be expanded in the normal waveguide modes and the expansion coefficients of all modes excited by the source (propagating and evanescent) are determined by the waveguide excitation theory.

Since the cylindrical waveguide used in this study has a finite length, the reflections due to the discontinuities at both ends also need to be considered and evaluated.

2.2.1 General Field Expressions in a Waveguide

Fig. 2.2 illustrates a waveguide of finite length in which a current source $\vec{J}_a$ is located in the region between z_1 and z_2. The total volume of the source region is V. S is defined as the total closed boundary surface of V and S_o is the total surface of conducting wall in V.

The fields excited by the source may be expressed as an infinite Fourier series in the orthogonal normal waveguide modes as follows:

$$\vec{E}_1 = \vec{E}_1^{+} + \vec{E}_1^{-} = \sum_q A_q \vec{E}_q^{+} + \sum_q B_q \vec{E}_q^{-} \qquad z < z_1 \qquad (2.1a)$$

$$\vec{H}_1 = \vec{H}_1^{+} + \vec{H}_1^{-} = \sum_q A_q \vec{H}_q^{+} + \sum_q B_q \vec{H}_q^{-} \qquad (2.1b)$$

$$\vec{E}_2 = \vec{E}_2^{+} + \vec{E}_2^{-} = \sum_q C_q \vec{E}_q^{+} + \sum_q D_q \vec{E}_q^{-} \qquad z > z_2 \tag{2.1c}$$

$$\vec{H}_2 = \vec{H}_2^{+} + \vec{H}_2^{-} = \sum_q C_q \vec{H}_q^{+} + \sum_q D_q \vec{H}_q^{-} \tag{2.1d}$$

where $$\vec{E}_q^{\pm} = (\vec{e}_q \pm \vec{e}_{zq})\, e^{\mp j\beta_q z} \tag{2.2a}$$

$$\vec{H}_q^{\pm} = (\pm \vec{h}_q + \vec{h}_{zq})\, e^{\mp j\beta_q z} \tag{2.2b}$$

In eqs. (2.1)and (2.2), q is a general summation index and implies a summation over all possible TE and TM modes, and the time dependence factor of $e^{j\omega t}$ has been suppressed. The β_q, e_q, e_{zq}, h_q and h_{zq} are the propagation constant, transverse and z-components of E fields, transverse and z- components of H fields for the q th waveguide mode, respectively. The super "+" and "-" indices represent the waves in positive and negative z directions, respectively. The unknown constants A_q, B_q, C_q and D_q are the expansion coefficients which are to be evaluated later.

We define reflection coefficients Γ_{1q} and Γ_{2q} as,

$$\Gamma_{1q} = \frac{A_q}{B_q} \tag{2.3a}$$

$$\Gamma_{2q} = \frac{D_q}{C_q} \tag{2.3b}$$

Substituting eqs. (2.2) and (2.3) into eq. (2.1), the following are obtained

$$\vec{E}_1 = \sum_q B_q \left[(\vec{e}_q - \vec{e}_{zq})\, e^{j\beta_q z} + \Gamma_{1q} (\vec{e}_q + \vec{e}_{zq}) e^{-j\beta_q z} \right] \qquad z < z_1 \tag{2.4}$$

$$\vec{H}_1 = \sum_q B_q[(-\vec{h}_q + \vec{h}_{zq})e^{j\beta_q z} + \Gamma_{1q}(\vec{h}_q + \vec{h}_{zq})e^{-j\beta_q z}] \quad z < z_1 \qquad (2.5)$$

$$\vec{E}_2 = \sum_q C_q[(\vec{e}_q + \vec{e}_{zq})e^{-j\beta_q z} + \Gamma_{2q}(\vec{e}_q - \vec{e}_{zq})e^{j\beta_q z}] \quad z > z_2 \qquad (2.6)$$

$$\vec{H}_2 = \sum_q C_q[(\vec{h}_q + \vec{h}_{zq})e^{-j\beta_q z} - \Gamma_{2q}(\vec{h}_q - \vec{h}_{zq})e^{j\beta_q z}] \quad z > z_2 \qquad (2.7)$$

2.2.2 Lorentz Lemma

Consider a volume region V bounded by a closed surface S as in Fig. 2.3. Let a current source $\vec{J}_a$ in V produce fields $\vec{E}_a$, $\vec{H}_a$, while a second source $\vec{J}_b$ produces fields $\vec{E}_b$, $\vec{H}_b$. The Lorentz Lemma states[6],

$$\int_v \nabla \cdot (\vec{E}_a \times \vec{H}_b - \vec{E}_b \times \vec{H}_a)dv = \int_v (\vec{E}_b \cdot \vec{J}_a - \vec{E}_a \cdot \vec{J}_b)dv \qquad (2.8)$$

With divergence theorem eq. (2.8) leads to

$$\oint_s (\vec{E}_a \times \vec{H}_b - \vec{E}_b \times \vec{H}_a) \cdot \hat{n}\, ds = \int_v (\vec{E}_b \cdot \vec{J}_a - \vec{E}_a \cdot \vec{J}_b)dv \qquad (2.9)$$

where S is the total surface enclosing V.

2.2.3 Excited Fields

In Fig. 2.2, let $\vec{E}_1$ and $\vec{E}_2$ be the $\vec{E}_a$, and $\vec{H}_1$ and $\vec{H}_2$ be the $\vec{H}_a$. These fields are produced by the current source $\vec{J}_a$ defined in the Lorentz Lemma. The $\vec{E}_b$ and $\vec{H}_b$ are assumed to be

$$\vec{E}_b = \vec{E}_q^- = (\vec{e}_q - \vec{e}_{zq})e^{j\beta_q z} \qquad (2.10a)$$

$$\vec{H}_b = \vec{H}_q^- = (-\vec{h}_q + \vec{h}_{zq})e^{j\beta_q z} \qquad (2.10b)$$

Both $\vec{E}_b$ and $\vec{H}_b$ are fields in a source-free region corresponding to $\vec{J}_b = 0$. Using Lorentz Lemma in our problem, V is assumed to be a region between z_1 and z_2, S is the total surface enclosing V and S_o is the total area of the conducting wall in region V. Eq. (2.9) can now be rewritten as follows:

$$\int_s (\vec{E}_a \times \vec{H}_q^- - \vec{E}_q^- \times \vec{H}_a) \cdot \hat{n}\, ds = \int_v \vec{E}_q^- \cdot \vec{J}_a\, dv$$

$$\int_{s_o} (\vec{E}_a \times \vec{H}_q^- - \vec{E}_q^- \times \vec{H}_a) \cdot \hat{n}\, ds + \int_{s-s_o} (\vec{E}_a \times \vec{H}_q^- - \vec{E}_q^- \times \vec{H}_a) \cdot \hat{n}\, ds$$

$$= \int_v \vec{E}_q^- \cdot \vec{J}_a\, dv \qquad (2.11)$$

The surface $S-S_o$ consists of two cross-sectional surfaces at z_1 and z_2. Since the boundary condition on the conducting wall S_o is $\hat{n} \times \vec{E}_a = \hat{n} \times \vec{E}_q^- = 0$, the first term of eq. (2.11) vanishes because

$$\int_{s_o} (\vec{E}_a \times \vec{H}_q^- - \vec{E}_q^- \times \vec{H}_a) \cdot \hat{n}\, ds = \int_{s_o} [(\hat{n} \times \vec{E}_a) \cdot \vec{H}_q^- - (\hat{n} \times \vec{E}_q^-) \cdot \vec{H}_a]\, ds = 0 \qquad (2.12)$$

Based on the power orthogonality property of the normal waveguide modes,

$$\int_{c.s.} \vec{E}_m^{\pm} \times \vec{H}_n^{\pm} \cdot \hat{n}\, ds = 0 \qquad n \neq m, \qquad (2.13)$$

eq. (2.11) leads to

$$\int_{s-s_o} (\vec{E}_a \times \vec{H}_q^- - \vec{E}_q^- \times \vec{H}_a) \cdot \hat{n}\, ds = \int_{z_1} (\vec{E}_a \times \vec{H}_q^- - \vec{E}_q^- \times \vec{H}_a) \cdot \hat{n}\, ds + \int_{z_2} (\vec{E}_a \times \vec{H}_q^- - \vec{E}_q^- \times \vec{H}_a) \cdot \hat{n}\, ds$$

$$= \int_{z_1} (\vec{E}_a \times \vec{H}_q^- - \vec{E}_q^- \times \vec{H}_a) \cdot (-\hat{z})\, ds + \int_{z_2} (\vec{E}_a \times \vec{H}_q^- - \vec{E}_q^- \times \vec{H}_a) \cdot (\hat{z})\, ds$$

$$= \int_{z_1} [\sum_p B_p (\vec{E}_p^- + \Gamma_{1p} \vec{E}_p^+) \times \vec{H}_q^- - \vec{E}_q^- \times \sum_p B_p (\vec{H}_p^- + \Gamma_{1p} \vec{H}_p^+)] \cdot (-\hat{z})\, ds$$

$$+ \int_{z_2} [\sum_p C_p (\vec{E}_p^+ + \Gamma_{2p} \vec{E}_p^-) \times \vec{H}_q^- - \vec{E}_q^- \times \sum_p C_p (\vec{H}_p^+ + \Gamma_{2p} \vec{H}_p^-)] \cdot (\hat{z})\, ds$$

$$= \int_{z_1} (-B_q \vec{E}_q^- \times \vec{H}_q^- - \Gamma_{1q} B_q \vec{E}_q^+ \times \vec{H}_q^- + B_q \vec{E}_q^- \times \vec{H}_q^- + B_q \Gamma_{1q} \vec{E}_q^- \times \vec{H}_q^+) \cdot \hat{z}\, ds$$

$$+ \int_{z_2} (C_q \vec{E}_q^+ \times \vec{H}_q^- + C_q \Gamma_{2q} \vec{E}_q^- \times \vec{H}_q^- - C_q \vec{E}_q^- \times \vec{H}_q^+ - C_q \Gamma_{2q} \vec{E}_q^- \times \vec{H}_q^-) \cdot \hat{z}\, ds$$

$$= B_q \Gamma_{1q} \int_{z_1} (\vec{E}_q^- \times \vec{H}_q^+ - \vec{E}_q^+ \times \vec{H}_q^-) \cdot \hat{z}\, ds + C_q \int_{z_2} (\vec{E}_q^+ \times \vec{H}_q^- - \vec{E}_q^- \times \vec{H}_q^+) \cdot \hat{z}\, ds$$

where $\int_{z_1} ds$ and $\int_{z_2} ds$ are the surface integrals over the cross sections at z_1 and z_2.

By substituting eq. (2.2) into the above equation, we get

$$\int_{s-s_o} (\vec{E}_a \times \vec{H}_q^- - \vec{E}_q^- \times \vec{H}_a) \cdot \hat{n}\, ds = B_q \Gamma_{1q} \int_{z_1} [(\vec{e}_q - \vec{e}_{zq}) \times (\vec{h}_q + \vec{h}_{zq}) - (\vec{e}_q + \vec{e}_{zq}) \times (-\vec{h}_q + \vec{h}_{zq})\ ] \cdot \hat{z}\, ds$$

$$+ C_q \int_{z_2} [(\vec{e}_q + \vec{e}_{zq}) \times (-\vec{h}_q + \vec{h}_{zq}) - (\vec{e}_q - \vec{e}_{zq}) \times (\vec{h}_q + \vec{h}_{zq})] \cdot \hat{z}\, ds$$

$$= (2 B_q \Gamma_{1q} - 2 C_q) \int_{c.s.} (\vec{e}_q \times \vec{h}_q) \cdot \hat{z}\, ds$$

or

$$2 (B_q \Gamma_{1q} - C_q) \int_{c.s.} (\vec{e}_q \times \vec{h}_q) \cdot \hat{z}\, ds = \int_v \vec{E}_q^- \cdot \vec{J}_a\, dv \qquad (2.14)$$

where $\int_{c.s.}$ ds is the surface integral over the cross-section of the waveguide and is independent of z.

Similarly, if $\vec{E}_q^+$ and $\vec{H}_q^+$ are chosen as the source-free region fields $\vec{E}_b$ and $\vec{H}_b$ corresponding to $\vec{J}_b = 0$, we obtain

$$2(C_q\Gamma_{2q} - B_q)\int_{c.s.} (\vec{e}_q \times \vec{h}_q)\cdot \hat{z}\, ds = \int_v \vec{E}_q^{\pm}\cdot \vec{J}_a\, dv \tag{2.15}$$

If M_q and N_q are defined as

$$M_q = \frac{\int_v \vec{E}_q^-\cdot \vec{J}_a\, dv}{2\int_{c.s.} (\vec{e}_q \times \vec{h}_q)\cdot \hat{z}\, ds} \tag{2.16a}$$

$$N_q = \frac{\int_v \vec{E}_q^+\cdot \vec{J}_a\, dv}{2\int_{c.s.} (\vec{e}_q \times \vec{h}_q)\cdot \hat{z}\, ds} \tag{2.16b}$$

then

$$\Gamma_{1q}B_q - C_q = M_q$$

$$\Gamma_{2q}C_q - B_q = N_q$$

or

$$B_q = \frac{\Gamma_{2q}M_q + N_q}{\Gamma_{1q}\Gamma_{2q} - 1} \tag{2.17a}$$

$$C_q = \frac{\Gamma_{1q}N_q + M_q}{\Gamma_{1q}\Gamma_{2q} - 1} \tag{2.17b}$$

The expansion coefficients for the EM field excited in the waveguide by a primary source are therefore determined in terms of the source current distribution $\vec{J}_a$ and the reflection coefficients Γ_{1q}, Γ_{2q}.

2.3 Calculation of Reflection Coefficients Γ_{1q} and Γ_{2q}

In section 2.2.1 and in Fig. 2.1, Γ_{1q} and Γ_{2q} have been defined as the reflection coefficients of q th waveguide mode due to the discontinuities at $z = -\ell_1$ and $z = \ell_2$, respectively. At $z = -\ell_1$, the waveguide is short-circuited by a good conductor. The $\vec{E}$ field in the region I of $z < 0$ is

$$\vec{E}_1 = \sum_q B_q [(\vec{e}_q - \vec{e}_{zq}) e^{j\beta_q z} + \Gamma_{1q} (\vec{e}_q + \vec{e}_{zq}) e^{-j\beta_q z}] \quad z < 0 \qquad (2.4)$$

Based on the boundary condition, $\hat{n} \times \vec{E}_1 = 0$, over the conducting wall, the transverse component of $\vec{E}_1$ at $z = -\ell_1$ vanishes. That is

$$\vec{E}_{1t}(z = -\ell_1) = \sum_q B_q (\vec{e}_q e^{-j\beta_q \ell_1} + \Gamma_{1q} \vec{e}_q e^{j\beta_q \ell_1}) = 0 \qquad (2.18)$$

The surface integral of the scalar product of $\vec{E}_{1t}$ and an arbitrary mode $\vec{e}_p$ over the short-circuited wall S_1 is also zero.

$$\int_{s_1} \vec{E}_{1t}(z = -\ell_1) \cdot \vec{e}_p \, ds = \int_{s_1} \sum_q B_q (e^{-j\beta_q \ell_1} + \Gamma_{1q} e^{j\beta_q \ell_1}) \vec{e}_q \cdot \vec{e}_p \, ds = 0$$

or
$$\sum_q B_q (e^{-j\beta_q \ell_1} + \Gamma_{1q} e^{j\beta_q \ell_1}) \int_{s_1} \vec{e}_q \cdot \vec{e}_p \, ds = 0 \qquad (2.19)$$

Due to the orthogonality of the waveguide modes, eq. (2.19) becomes

$$B_q (e^{-j\beta_p \ell_1} + \Gamma_{1p} e^{j\beta_p \ell_1}) \int_{s_1} \vec{e}_p \cdot \vec{e}_p \, ds = 0 \qquad (2.20)$$

Since B_q and $\int_{s_1} \vec{e}_p \cdot \vec{e}_p \, ds$ are both non-zero constants, it leads to

$$e^{-j\beta_p \ell_1} + \Gamma_{1p} e^{j\beta_p \ell_1} = 0$$

where p represents an arbitrary mode. Thus, the reflection coefficient due to the short-circuit discontinuity at $z = -\ell_1$ (referred to $z = 0$) is

$$\Gamma_{1q} = -e^{-j2\beta_q \ell_1} \tag{2.21}$$

The calculation of Γ_{2q}, the reflection coefficient due to the open-end discontinuity at $z = \ell_2$, is much more complicated than Γ_{1q}. The diffraction effects which are due fundamentally to the fact that the sources are distributed over an open surface, can cause the regenerations of other waveguide modes. This coupling phenomenon which can be handled by a ray-optical theory[7] is extremely complicated and not appropriate for the present analysis.

Fortunately, the experiment and also the ray-optical theory indicate that whenever the dimensions of the aperture are not small compared with the wavelength, which happen to be our case, the diffraction effect is insignificant and the major portion of the aperture field is due to the field from the waveguide[8]. An accurate reflection coefficient at the open-end can only be determined by extremely complicated methods[7, 9]. Since the reflection coefficient at a large aperture is usually small, a simple method based on transmission line principle will be employed to calculate the reflection coefficient. Assume that the reflection coefficient for the qth mode at the open-end, $z = \ell_2$, is k_{2q} and it is defined as the ratio of $(e_q)_r / (e_q)_i$ or the ratio of the transverse components of the

reflected and incident electric field vectors. When extrapolated to the plane of the open-end, k_{2q} can be interpreted as, [8]

$$k_{2q} = \frac{\zeta_o - Z_q}{\zeta_o + Z_q} \tag{2.22}$$

where ζ_o and Z_q are the field impedances of space and qth mode, respectively. The transverse component of electric field in the region II of $z > 0$ is

$$\vec{E}_{2t} = \sum_q C_q (\vec{e}_q e^{-j\beta_q z} + \Gamma_{2q} \vec{e}_q e^{j\beta_q z}) \tag{2.23}$$

At $z = \ell_2$ or the open end,

$$\text{The incident wave} = \sum_q C_q \vec{e}_q (r,\phi) e^{-j\beta_q \ell_2}$$

$$\text{The reflected wave} = \sum_q C_q \Gamma_{2q} \vec{e}_q (r,\phi) e^{j\beta_q \ell_2}$$

By the definition of k_{2q}, the reflected wave is equal to

$$\sum_q C_q \Gamma_{2q} \vec{e}_q (r,\phi) e^{j\beta_q \ell_2} = \sum_q C_q k_{2q} \vec{e}_q (r,\phi) e^{-j\beta_q \ell_2}$$

or
$$\sum_q C_q (\Gamma_{2q} e^{j\beta_q \ell_2} - k_{2q} e^{-j\beta_q \ell_2}) \vec{e}_q (r,\phi) = 0 \tag{2.24}$$

If $\vec{e}_p$ is the transverse component of the electric field vector of an arbitrary p th mode, the surface integration of the product of $\vec{e}_p$ and eq. (2.24) over the waveguide open-end S_2 should also be zero, that is

$$\int_{S_2} [\sum_q C_q (\Gamma_{2q} e^{j\beta_q \ell_2} - k_{2q} e^{-j\beta_q \ell_2}) \vec{e}_q] \cdot \vec{e}_p \, ds = 0$$

or $$\sum_q C_q(\Gamma_{2q} e^{j\beta_q \ell_2} - k_{2q} e^{-j\beta_q \ell_2}) \int_{s_2} \vec{e}_p \cdot \vec{e}_p \, ds = 0$$

$$C_p(\Gamma_{2p} e^{j\beta_p \ell_2} - k_{2p} e^{-j\beta_p \ell_2}) \int_{s_2} \vec{e}_p \cdot \vec{e}_p \, ds = 0 \qquad (2.25)$$

Eq. (2.25) has been derived with the help of the orthogonality property of the waveguide modes. Since C_p and $\int_{s_2} \vec{e}_p \cdot \vec{e}_p \, ds$ are non-zero constants, eq. (2.25) leads to

$$\Gamma_{2q} e^{j\beta_q \ell_2} - k_{2q} e^{-j\beta_q \ell_2} = 0$$

or

$$\Gamma_{2q} = k_{2q} e^{-j2\beta_q \ell_2} = \frac{\zeta_o - Z_q}{\zeta_o + Z_q} e^{-j2\beta_q \ell_2} \qquad (2.26)$$

Γ_{2q} is the reflection coefficient of the q th mode at z=0 due to the open-end at $z = \ell_2$.

2.4 Input Resistance of the Primary Radiator

The input resistance R_{in} of the primary radiator is defined at the terminals of the primary radiator and is equal to the total real power radiated divided by one half of the square of the input current of the primary radiator. The real power radiated from the exciter can be obtained by calculating the real part of the complex Poynting vector of the propagating modes. That is

$$P = \frac{1}{2} \mathrm{Re} \int_{c.s.} (\vec{E}_2 \times \vec{H}_2^*) \cdot \hat{z} \, ds \quad \text{for propagating modes only} \qquad (2.27)$$

Substituting eqs. (2.6) and (2.7) into eq. (2.27), and taking advantage of waveguide orthogonality, P is obtained as

$$P = \frac{1}{2} \mathrm{Re} \int_{c.s.} [\sum_q C_q(\vec{E}_q^+ + \Gamma_{2q}\vec{E}_q^-)] \times [\sum_{q'} C_{q'}(\vec{H}_{q'}^+ + \Gamma_{2q}\vec{H}_{q'}^-)]^* \cdot \hat{z}\, ds$$

$$= \frac{1}{2} \sum_q |C_p|^2 \mathrm{Re} \int_{c.s.} [(\vec{E}_q^+ + \Gamma_{2q}\vec{E}_q^-) \times (\vec{H}_q^+ + \Gamma_{2q}\vec{H}_q^-)^*] \cdot \hat{z}\, ds$$

$$= \frac{1}{2} \sum_q |C_q|^2 \mathrm{Re}(1 - |\Gamma_{2q}|^2 + \Gamma_{2q} e^{j2\beta_q z} - \Gamma_{2q}^* e^{-j2\beta_q z}) \int_{c.s.} \frac{1}{Z_q} (\vec{e}_q \cdot \vec{e}_q) ds$$

where q are for those propagating modes only. Because only the propagating modes have been considered, the wave impedance and $\vec{e}_q$ are real, and $\mathrm{Re}[\Gamma_{2q} e^{j2\beta_q z} - (\Gamma_{2q} e^{j2\beta_q z})^*] = 0$, therefore

$$P = \frac{1}{2} \sum_q \frac{|C_q|^2}{Z_q} (1 - |\Gamma_{2q}|^2) \int_{c.s.} (\vec{e}_q \cdot \vec{e}_q) ds \qquad (2.28)$$

The input resistance of the primary radiator, R_{in}, is then defined as

$$R_{in} = \frac{2P}{I_o I_o^*} = \frac{1}{I_o I_o^*} \sum_q \frac{|C_q|^2}{Z_q} (1 - |\Gamma_{2q}|^2) \int_{c.s.} (\vec{e}_q \cdot \vec{e}_q) ds. \qquad (2.29)$$

The reactive component of the input impedance was attempted with an induced EMF method without much success. The reason is that there are infinite number of higher order, cut-off modes present on the exciter surface and it is hard to obtain a sensible and accurate reactance.

2.5 Radiation Fields of the Open-Cavity Antenna

The radiation fields of an open-cavity radiator are calculated based on the aperture fields at the open-end of the cavity.

2.5.1 Geometry and General Expressions for the Radiation Fields

Figure 2.4 shows the geometry of the problem. The x'-y' plane is the aperture plane and s' is the surface which forms the aperture. The radiation fields are maintained by the aperture

fields $\vec{E}_a$ and $\vec{H}_a$. Spherical coordinates (r, θ, ϕ) are adopted to respresent the radiation fields, while the aperture fields are expressed in terms of cylindrical coordinates (r', ϕ', ℓ_2). $P(r, \theta, \phi)$ is an arbitrary observation point in the radiation zone and $P'(r', \phi', \ell_2)$ is a point on the aperture. The distance between P and P' is $R = |\vec{r} - \vec{r}'|$ and the radiation zone approximation for R is

$$R = \begin{cases} r - \vec{r}' \cdot \hat{r} & \text{--- for phase terms} \\ r & \text{--- for amplitude terms} \end{cases} \qquad (2.30)$$

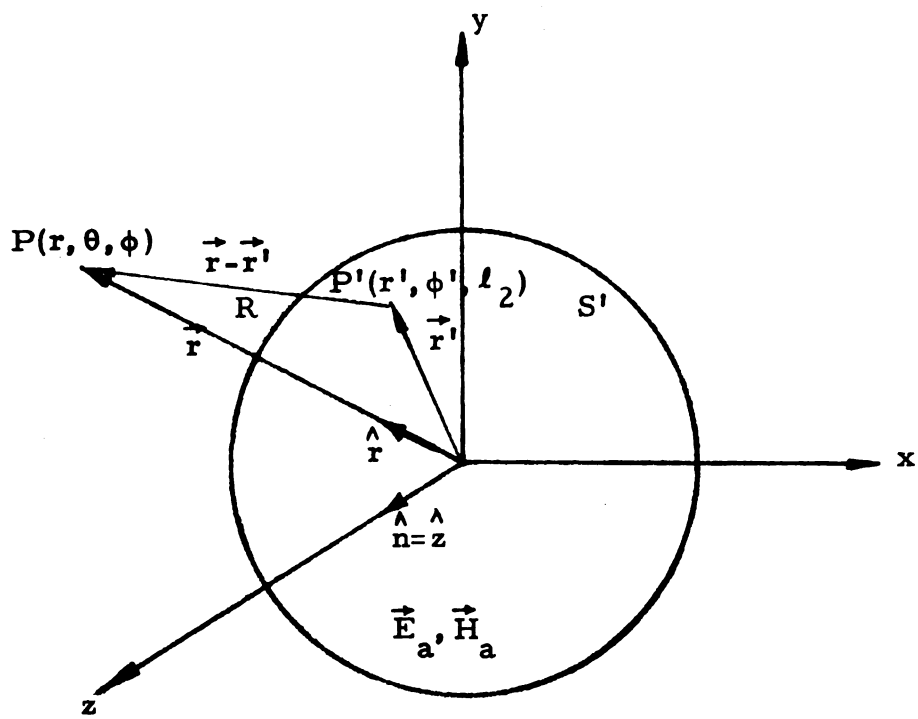

Fig. 2.4 Geometry for calculation of the radiation fields

The radiation fields at $P(\vec{r})$ maintained by the aperture fields $\vec{E}_a$ and $\vec{H}_a$ are given by[10]

$$E_\theta^r = -\frac{jk_o}{4\pi}\frac{e^{-jk_o r}}{r}(L_\phi^r + \zeta_o N_\theta^r) \tag{2.31a}$$

$$E_\phi^r = \frac{jk_o}{4\pi}\frac{e^{-jk_o r}}{r}(L_\theta^r - \zeta_o N_\phi^r) \tag{2.31b}$$

where

$$\vec{N}^r(\vec{r}) = \int_{s'} \hat{n} \times \vec{H}_a(\vec{r}\,') e^{jk_o \vec{r}\,' \cdot \hat{r}}\, ds' \tag{2.32a}$$

$$\vec{L}^r(\vec{r}) = \int_{s'} -\hat{n} \times \vec{E}_a(\vec{r}\,') e^{jk_o \vec{r}\,' \cdot \hat{r}}\, ds' \tag{2.32b}$$

$$\vec{E}_a(\vec{r}\,') = \hat{r}' E_{ar}(\vec{r}\,') + \hat{\phi}' E_{a\phi}(\vec{r}\,') \tag{2.32c}$$

$$\vec{H}_a(\vec{r}\,') = \hat{r} H_{ar}(\vec{r}\,') + \hat{\phi}' H_{a\phi}(\vec{r}\,') \tag{2.32d}$$

Since the aperture fields $\vec{E}_a$ and $\vec{H}_a$ may consist of all possible TE and TM modes, all exicted modes should be considered.

In section 2.3, the diffraction and coupling effects at the aperture have been neglected, therefore the superposition method will be employed to obtain the total radiation fields by summing up the radiation fields maintained by the aperture fields of all excited modes.

The unit normal vector $\hat{n}$ on the aperture is $\hat{z}'$, therefore eqs. (2.32) for the q th mode yield the following:

$$\vec{L}_q^r(\vec{r}) = -\int_{s'} \hat{z}' \times [\hat{r}' E_{ar}(\vec{r}') + \hat{\phi}' E_{a\phi}(\vec{r}')] e^{jk_o \vec{r}' \cdot \hat{r}} ds'$$

$$= \int_{s'} [\hat{r}' E_{a\phi}(\vec{r}') - \hat{\phi}' E_{ar}(\vec{r}')] e^{jk_o r' \hat{r}' \cdot \hat{r}} ds' \qquad (2.33a)$$

$$\vec{N}_q^r(\vec{r}) = \int_{s'} \hat{z} \times \frac{1}{Z_q} [\hat{z} \times \vec{E}_a(\vec{r}')] e^{jk_o \vec{r}' \cdot \hat{r}} ds'$$

$$= -\int_{s'} \frac{1}{Z_q} [\hat{r}' E_{ar}(\vec{r}') + \hat{\phi}' E_{a\phi}(\vec{r}')] e^{jk_o r' \hat{r}' \cdot \hat{r}} ds' \qquad (2.33b)$$

The expressions of unit vectors $\hat{r}'$ and $\hat{\phi}'$ in terms of spherical coordinates (r, θ, ϕ) are

$$\hat{r}' = \hat{r} \sin\theta \cos(\phi - \phi') + \hat{\theta} \cos\theta \cos(\phi - \phi') - \hat{\phi} \sin(\phi - \phi') \qquad (2.34a)$$

$$\hat{\phi}' = \hat{r} \sin\theta \sin(\phi - \phi') + \hat{\theta} \cos\theta \sin(\phi - \phi') + \hat{\phi} \cos(\phi - \phi') \qquad (2.34b)$$

Therefore

$$N_q^r(\vec{r}) = -\int_{s'} \frac{1}{Z_q} [E_{ar}(\vec{r}')\{\hat{r} \sin\theta \cos(\phi - \phi') + \hat{\theta} \cos\theta \cos(\phi - \phi')$$

$$- \hat{\phi} \sin(\phi - \phi')\} + E_{a\phi}(\vec{r}')\{\hat{r} \sin\theta \sin(\phi - \phi') + \hat{\theta} \cos\theta \sin(\phi - \phi')$$

$$+ \hat{\phi} \cos(\phi - \phi')\}] e^{jk_o r' \sin\theta \cos(\phi - \phi')} ds' \qquad (2.35a)$$

$$\vec{L}_q^r(\vec{r}) = \int_{s'} [E_{a\phi}(\vec{r}')\{\hat{r} \sin\theta \cos(\phi - \phi') + \hat{\theta} \cos\theta \cos(\phi - \phi') - \hat{\phi} \sin(\phi - \phi')\}$$

$$- E_{ar}(\vec{r}')\{\hat{r} \sin\theta \sin(\phi - \phi') + \hat{\theta} \cos\theta \sin(\phi - \phi') + \hat{\phi} \cos(\phi - \phi')\}]$$

$$e^{jk_o r' \sin\theta \cos(\phi - \phi')} ds' \qquad (2.35b)$$

The $N_{\theta q}^r$, $N_{\phi q}^r$, $L_{\theta q}^r$ and $L_{\phi q}^r$ are then determined,

$$N_{\theta q}^{r}(\vec{r}) = -\cos\theta \int_{s'} \frac{1}{Z_q}\left[E_{ar}(\vec{r}')\cos(\phi-\phi') + E_{a\phi}(\vec{r}')\sin(\phi-\phi')\right] \cdot e^{jk_o r'\sin\theta\cos(\phi-\phi')}\, ds' \tag{2.36a}$$

$$N_{\phi q}^{r}(\vec{r}) = -\int_{s'} \frac{1}{Z_q}\left[E_{a\phi}(\vec{r}')\cos(\phi-\phi') - E_{ar}(\vec{r}')\sin(\phi-\phi')\right] e^{jk_o r'\sin\theta\cos(\phi-\phi')}\, ds' \tag{2.36b}$$

$$L_{\theta q}^{r}(\vec{r}) = \cos\theta \int_{s'} \left[E_{a\phi}(\vec{r}')\cos(\phi-\phi') - E_{ar}(\vec{r}')\sin(\phi-\phi')\right] \cdot e^{jk_o r'\sin\theta\cos(\phi-\phi')}\, ds' \tag{2.36c}$$

$$L_{\phi q}^{r}(\vec{r}) = -\int_{s'} \left[E_{ar}(\vec{r}')\cos(\phi-\phi') + E_{a\phi}(\vec{r}')\sin(\phi-\phi')\right] \cdot e^{jk_o r'\sin\theta\cos(\phi-\phi')}\, ds' \tag{2.36d}$$

Therefore the radiation fields maintained by the q th mode of the aperture field are

$$E_{\theta q}^{r}(\vec{r}) = \frac{jk_o}{4\pi}\frac{e^{-jk_o r}}{r} \int_{s'} (1 + \frac{\zeta_o}{Z_q}\cos\theta)\left[E_{ar}(\vec{r}')\cos(\phi-\phi') + E_{a\phi}(\vec{r}')\sin(\phi-\phi')\right] e^{jk_o r'\sin\theta\cos(\phi-\phi')}\, ds' \tag{2.37a}$$

$$E_{\phi q}^{r}(\vec{r}) = \frac{jk_o}{4\pi}\frac{e^{-jk_o r}}{r} \int_{s'} (\frac{\zeta_o}{Z_q} + \cos\theta)\left[E_{a\phi}(\vec{r}')\cos(\phi-\phi') - E_{ar}(\vec{r}')\sin(\phi-\phi')\right] \cdot e^{jk_o r'\sin\theta\cos(\phi-\phi')}\, ds' \tag{2.37b}$$

From eq. (2.23), the transverse component of $\vec{E}_2$ at $z = \ell_2$ is

$$\vec{E}_{2t}(z=\ell_2) = \sum_q C_q (e^{-j\beta_q \ell_2} + \Gamma_{2q} e^{j\beta_q \ell_2})\vec{e}_q \tag{2.38}$$

Then E_{ar} and $E_{a\phi}$ of the q th mode can be found as

$$E_{ar}(r', \phi') = C_q(e^{-j\beta_q \ell_2} + \Gamma_{2q} e^{j\beta_q \ell_2}) e_{rq}(r', \phi') \qquad (2.39a)$$

$$E_{a\phi}(r', \phi') = C_q(e^{-j\beta_q \ell_2} + \Gamma_{2q} e^{j\beta_q \ell_2}) e_{\phi q}(r', \phi') \qquad (2.39b)$$

Substituting eqs. (2.39) into eqs. (2.37) and with (2.38), the following are obtained:

$$E_\theta^r(r) = \frac{jk_o}{4\pi} \frac{e^{-jk_o r}}{r} \sum_q C_q(1 + \frac{\zeta_o}{Z_q} \cos\theta)(e^{-j\beta_q \ell_2} + \Gamma_{2q} e^{j\beta_q \ell_2}) F_{\theta q}(\theta, \phi) \qquad (2.40a)$$

$$E_\phi^r(r) = \frac{jk_o}{4\pi} \frac{e^{-jk_o r}}{r} \sum_q C_q(\frac{\zeta_o}{Z_q} + \cos\theta)(e^{-j\beta_q \ell_2} + \Gamma_{2q} e^{j\beta_q \ell_2}) F_{\phi q}(\theta, \phi) \qquad (2.40b)$$

where

$$F_{\theta q}(\theta, \phi) = \int_o^a \int_{-\pi}^{\pi} [e_{rq}(r', \phi')\cos(\phi - \phi') + e_{\phi q}(r', \phi')\sin(\phi - \phi')] \cdot e^{jzr'\cos(\phi - \phi')} r' d\phi' dr' \qquad (2.41a)$$

$$F_{\phi q}(\theta, \phi) = \int_o^a \int_{-\pi}^{\pi} [e_{\phi q}(r', \phi')\cos(\phi - \phi') - e_{rq}(r', \phi')\sin(\phi - \phi')] \cdot e^{jzr'\cos(\phi - \phi')} r' d\phi' dr' \qquad (2.41b)$$

$$z = k_o \sin\theta \qquad (2.41c)$$

2.5.2 Evaluation of $F_{\theta q}(\theta, \phi)$ and $F_{\phi q}(\theta, \phi)$ for TE Modes

The Appendix gives the normal TE mode expressions. Without losing the generality, we choose the e_{rq} and $e_{\phi q}$ as follows:

$$e_{rq}(r', \phi') = \frac{n}{k_{cq}} \frac{J_n(k_{cq} r')}{r'} \sin n\phi' \qquad (2.42a)$$

$$e_{\phi q}(r', \phi') = J_n'(k_{cq} r') \cos n\phi' \qquad (2.42b)$$

The Bessel function satisfies the following recurrence relations

$$J'_m(z) = \frac{m}{z} J_m(z) - J_{m+1}(z) = \frac{1}{2}[J_{m-1}(z) - J_{m+1}(z)] = -\frac{m}{z} J_m(z) + J_{m-1}(z) \tag{2.43a}$$

$$\frac{m}{z} J_m(z) = \frac{1}{2}[J_{m+1}(z) + J_{m-1}(z)] \tag{2.43b}$$

Therefore the e_{rq} and $e_{\phi q}$ can be stated as

$$e_{rq}(r', \phi') = \frac{1}{2}[J_{n-1}(k_{cq}r') + J_{n+1}(k_{cq}r')] \sin n\phi' \tag{2.44a}$$

$$e_{\phi q}(r', \phi') = \frac{1}{2}[J_{n-1}(k_{cq}r') - J_{n+1}(k_{cq}r')] \cos n\phi' \tag{2.44b}$$

and

$$e_{rq}\cos(\phi-\phi') + e_{\phi q}\sin(\phi-\phi')$$

$$= \frac{1}{2}[J_{n-1}(k_{cq}r')\{\sin n\phi'\cos(\phi-\phi') + \cos n\phi'\sin(\phi-\phi')\} + J_{n+1}(k_{cq}r') \{\sin n\phi'\cos(\phi-\phi') - \cos n\phi'\sin(\phi-\phi')\}]$$

$$= \frac{1}{2}[J_{n-1}(k_{cq}r')\sin\{(n-1)\phi'+\phi\} + J_{n+1}(k_{cq}r')\sin\{(n+1)\phi'-\phi\}] \tag{2.45}$$

With the help of the Bessel-Fourier series, we have

$$e^{jzr'\cos(\phi-\phi')} = J_o(zr') + \sum_{n=1}^{\infty} 2j^n J_n(zr')\cos n(\phi-\phi') \tag{2.46}$$

Also $\int_{-\pi}^{\pi} \sin mx \cos nx\, dx = 0$

$$\int_{-\pi}^{\pi} \sin mx \sin nx\, dx = \int_{-\pi}^{\pi} \cos mx \cos nx\, dx = 0 \quad \text{for } m \neq n$$

$$\int_{-\pi}^{\pi} \sin^2 mx\, dx = \int_{-\pi}^{\pi} \cos^2 mx\, dx = \pi$$

By substituting eqs. (2.45), (2.46) and the above eqs. into $F_{\theta q}$, it becomes

$$F_{\theta q} = \frac{1}{2} \int_0^A \int_{-\pi}^{\pi} [J_{n-1}(k_{cq} r')\sin\{(n-1)\phi'+\phi\} + J_{n+1}(k_{cq} r')\sin\{(n+1)\phi'-\phi\}] \cdot$$

$$[J_o(zr') + \sum_{m=1}^{\infty} 2j^m J_m(zr')\cos m(\phi-\phi')] \cdot r' d\phi' dr'$$

$$= \pi j^{n-1} \sin n\phi \int_0^A [J_{n-1}(k_{cq} r') J_{n-1}(zr') - J_{n+1}(k_{cq} r') J_{n+1}(k_{cq} r')]$$

$$\cdot r' dr' \qquad (2.47)$$

The Lommel integral formula gives

$$\int_0^x x J_n(\alpha x) J_n(\beta x) dx = \frac{x}{\alpha^2 - \beta^2} [J_n(\alpha x) \frac{d}{dx} J_n(\beta x) - J_n(\beta x) \frac{d}{dx} J_n(\alpha x)] \qquad (2.48)$$

Eq. (2.48) and the recurrence relations are used to lead to

$$\int_0^A J_{n-1}(k_{cq} r') J_{n-1}(zr') r' dr'$$

$$= \frac{A}{k_{cq}^2 - z^2} [J_{n-1}(k_{cq} A) z J'_{n-1}(zA) - J_{n-1}(zA) k_{cq} J'_{n-1}(k_{cq} A)]$$

$$= \frac{A}{k_{cq}^2 - z^2} [k_{cq} J_n(k_{cq} A)\{\frac{2n}{zA} J_n(zA) - J_{n+1}(zA)\} - z J_n(zA) \cdot$$

$$\{\frac{2n}{k_{cq} A} J_n(k_{cq} A) - J_{n+1}(k_{cq} A)\}] \qquad (2.49)$$

$$\int_0^A J_{n+1}(k_{cq} r') J_{n+1}(zr') r' dr'$$

$$= \frac{A}{k_{cq}^2 - z^2} [J_{n+1}(k_{cq} A) z J'_{n+1}(zA) - J_{n+1}(zA) k_{cq} J'_{n+1}(k_{cq} A)]$$

$$= \frac{A}{k_{cq}^2 - z^2} [J_{n+1}(k_{cq} A) z J_n(zA) - J_{n+1}(zA) k_{cq} J_n(k_{cq} A)] \qquad (2.50)$$

With eqs. (2.49) and (2.50), $F_{\theta q}$ becomes

$$F_{\theta q}(\theta, \phi) = j^{n-1} \frac{2n\pi \sin n\phi}{k_{cq}\beta_o \sin\theta} J_n(\beta_o A \sin\theta) J_n(k_{cq}A) \qquad (2.51)$$

In calculating $F_{\phi q}(\theta, \phi)$, the same procedure is followed as for the case of $F_{\theta q}$.

$$e_{\phi q}\cos(\phi-\phi') - e_{rq}\sin(\phi-\phi') = \frac{1}{2}[J_{n-1}(k_{cq}r')\cos\{(n-1)\phi'+\phi\} - J_{n+1}(k_{cq}r')\cos\{(n+1)\phi'-\phi\}]$$

$$F_{\phi q} = \frac{1}{2}\int_o^A \int_{-\pi}^{\pi} [J_{n-1}(k_{cq}r')\cos\{(n-1)\phi'+\phi\} - J_{n+1}(k_{cq}r')\cos\{(n+1)\phi'-\phi\}] \cdot [J_o(zr') + \sum_{m=1}^{\infty} 2j^m J_m(zr')\cos m(\phi-\phi')]\, r'd\phi'dr'$$

$$F_{\phi q} = j^{n-1}\pi\cos n\phi \int_o^A [J_{n-1}(k_{cq}r')J_{n-1}(zr') + J_{n+1}(k_{cq}r')J_{n+1}(zr')]\, r'dr' \qquad (2.52)$$

The integration of eq. (2.52) will be carried out differently in order to take advantage of $J'_n(k_{cq}A) = 0$.

$$\int_o^A J_{n-1}(k_{cq}r')J_{n-1}(zr')r'dr'$$

$$= \frac{A}{k_{cq}^2 - z^2}\left[k_{cq}J_n(k_{cq}A)\left\{J'_n(zA) + \frac{n}{zA}J_n(zA)\right\} - zJ_n(zA)\left\{J'_n(k_{cq}A) + \frac{n}{k_{cq}A}J_n(zA)\right\}\right] \qquad (2.53)$$

$$\int_o^A J_{n+1}(k_{cq}r')J_{n+1}(zr')r'dr'$$

$$= \frac{A}{k_{cq}^2 - z^2}\left[z\left\{\frac{n}{k_{cq}A}J_n(k_{cq}A) - J'_n(k_{cq}A)\right\}J_n(zA) - k_{cq}\left\{\frac{n}{zA}J_n(zA) - J'_n(zA)\right\}J_n(k_{cq}A)\right] \qquad (2.54)$$

By substituting eqs. (2.53) and (2.54) into eq. (2.52), the final expression becomes

$$F_{\phi q}(\theta, \phi) = j^{n-1} \frac{2\pi A k_{cq} \cos n\phi}{k_{cq}^2 - (\beta_o \sin\theta)^2} J_n(k_{cq}A) J_n'(\beta_o A \sin\theta) \qquad (2.55)$$

2.5.3 Evaluation of $F_{\theta q}(\theta, \phi)$ and $F_{\phi q}(\theta, \phi)$ for TM Modes

The following field expressions are appropriate for the TM modes:

$$e_{rq}(r', \phi') = J_n'(k_{cq} r') \sin n\phi' \qquad (2.56a)$$

$$e_{\phi q}(r', \phi') = \frac{n}{k_{cq} r} J_n(k_{cq} r') \cos n\phi' \qquad (2.56b)$$

Application of the recursion formulas leads to the alternate expression

$$e_{rq}\cos(\phi-\phi') + e_{\phi q}\sin(\phi-\phi')$$

$$= \frac{1}{2}\Big[\{J_{n-1}(k_{cq}r') - J_{n+1}(k_{cq}r')\} \sin(n\phi')\cos(\phi-\phi') + \{J_{n+1}(k_{cq}r') + J_{n-1}(k_{cq}r')\} \cos(n\phi')\sin(\phi-\phi')\Big]$$

$$= \frac{1}{2}\Big[J_{n-1}(k_{cq}r')\sin\{(n-1)\phi'+\phi\} - J_{n+1}(k_{cq}r')\sin\{(n+1)\phi'-\phi\}\Big] \qquad (2.57)$$

Substituting eqs. (2.57) and Bessel-Fourier series into $F_{\theta q}$ and results in

$$F_{\theta q} = j^{n-1} \pi \sin(n\phi) \int_o^A \Big[J_{n-1}(k_{cq}r') J_{n-1}(zr') + J_{n+1}(k_{cq}r') J_{n+1}(zr')\Big] r'dr' \qquad (2.58)$$

From eqs. (2.53), (2.54) and the boundary condition of $J_n(k_{cq}A) = 0$ for TM modes

$$F_{\theta q}(\theta, \phi) = j^{n+1} \frac{2\pi\beta_o A \sin\theta \sin n\phi}{k_{cq}^2 - (\beta_o \sin\theta)^2} J_n(\beta_o A \sin\theta) J_n'(k_{cq}A) \qquad (2.59)$$

Similarly, $F_{\phi q}(\theta, \phi)$ for TM modes can be evaluated as

$$F_{\phi q}(\theta, \phi) = j^{n-1} \pi \cos n\phi \int_0^A [\, J_{n-1}(k_{cq} r') J_{n-1}(zr') - J_{n+1}(k_{cq} r') J_{n+1}(zr')] \, r' dr'$$

$$= j^{n-1} \frac{2 n \pi \cos n\phi}{z k_{cq}} J_n(k_{cq} A) J_n(zA) = 0 \qquad (2.60)$$

2.5.4 Modified $F_{\theta q}(\theta, \phi)$ and $F_{\phi q}(\theta, \phi)$

In the Appendix, there are two sets of waveguide mode expressions for both TE and TM modes. The reason for keeping both sets is that for some configurations of primary exciters both sets of waveguide modes may all be excited. In the course of calculating expansion coefficient C_q, the proper set of waveguide modes is picked according to the geometry of the primary radiator. Since both sets of the waveguide modes may possibly be excited, it is also necessary to calculate the $F_{\theta q}$ and $F_{\phi q}$ for the second set of waveguide modes since these are not covered in the two previous sections.

The modified TE modes have the following forms

$$e_{rq}(r', \phi') = - \frac{n}{k_{cq} r'} J_n(k_{cq} r') \cos n\phi' \qquad (2.61a)$$

$$e_{\phi q}(r', \phi') = J_n'(k_{cq} r') \sin n\phi' \qquad (2.61b)$$

and the modified $F_{\theta q}(\theta, \phi)$ and $F_{\phi q}(\theta, \phi)$ can be evaluated to be

$$F_{\theta q}(\theta,\phi) = j^{n+1}\frac{2n\pi\cos(n\phi)}{k_{cq}\beta_o\sin\theta}J_n(\beta_o A\sin\theta)J_n(k_{cq}A) \tag{2.62}$$

$$F_{\phi q}(\theta,\phi) = j^{n-1}\frac{2\pi AK_{cq}\sin(n\phi)}{k_{cq}^2-(\beta_o\sin\theta)^2}J_n(k_{cq}A)J_n'(\beta_o A\sin\theta) \tag{2.63}$$

For the TM modes with the following expressions,

$$e_{rq}(r',\phi') = -J_n'(k_{cq}r')\cos(n\phi') \tag{2.64a}$$

$$e_{\phi q}(r',\phi') = \frac{n}{k_{cq}r'}J_n(k_{cq}r')\sin(n\phi') \tag{2.64b}$$

the modified radiation fields are calculated to be

$$F_{\theta q}(\theta,\phi) = j^{n-1}\frac{2\pi\beta_o A\sin\theta\cos(n\phi)}{k_{cq}^2-\beta_o^2\sin^2\theta}J_n(\beta_o A\sin\theta)J_n'(k_{cq}A) \tag{2.65}$$

$$F_{\phi q}(\theta,\phi) = j^{n-1}\frac{2n\pi\sin n\phi}{k_{cq}\beta_o\sin\theta}J_n(k_{cq}A)J_n(\beta_o A\sin\theta) = 0 \tag{2.66}$$

2.5.5 Radiation Fields Due to the Individual Waveguide Modes

The radiation field $\vec{E}^r$ in eqs. (2.40) can be rearranged as follows:

$$E_\theta^r(r,\theta,\phi) = \frac{jk_o}{4\pi}\frac{e^{-jk_o r}}{r}\sum_q C_q(e^{-j\beta_q\ell_2}+\Gamma_{2q}e^{j\beta_q\ell_2})I_{\theta q}(\theta,\phi) \tag{2.67a}$$

$$E_\phi^r(r,\theta,\phi) = \frac{jk_o}{4\pi}\frac{e^{-jk_o r}}{r}\sum_q C_q(e^{-j\beta_q\ell_2}+\Gamma_{2q}e^{j\beta_q\ell_2})I_{\phi q}(\theta,\phi) \tag{2.67b}$$

where $I_{\theta q}(\theta,\phi) = (1+\frac{\zeta_o}{Z_q}\cos\theta)F_{\theta q}(\theta,\phi)$ (2.67c)

$$I_{\phi q}(\theta,\phi) = (\frac{\zeta_o}{Z_q}+\cos\theta)F_{\phi q}(\theta,\phi) \tag{2.67d}$$

$I_{\theta q}$ and $I_{\phi q}$ are defined as the q th waveguide mode radiation pattern functions, since they describe the θ and ϕ dependence of the radiation field E^r.

Figures (2.5) and (2.6) show some of the radiation patterns in the E-plane ($\phi = \frac{\pi}{2}$) and H-plane ($\phi = 0$) for TE and TM modes, respectively. These patterns are calculated from the pattern functions $I_{\theta q}$ and $I_{\phi q}$, for the case of radius A equal to λ_o or one free-space wavelength.

The solid line represents the E-plane pattern while the dotted line indicates the H-plane pattern.

In Fig. 2.5(c), the H-plane radiation pattern of the TE_{21} mode is same as that of the E-plane. In Fig. 2.6, the E-plane and H-plane radiation patterns for the TM_{01} mode are identical, and the H-plane field patterns for both TM_{11} and TM_{12} modes are zero.

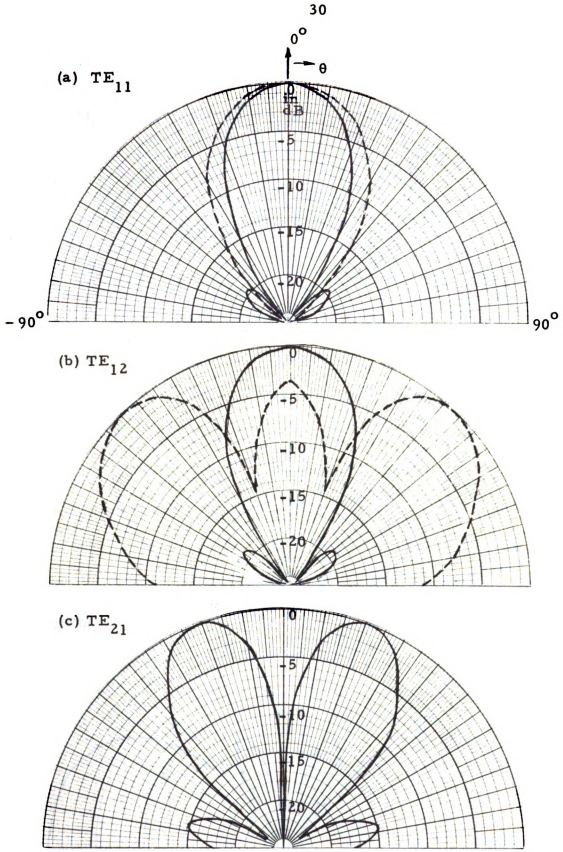

Fig. 2.5 Radiation patterns for (a) TE_{11} mode, (b) TE_{12} mode, (c) TE_{21} mode.

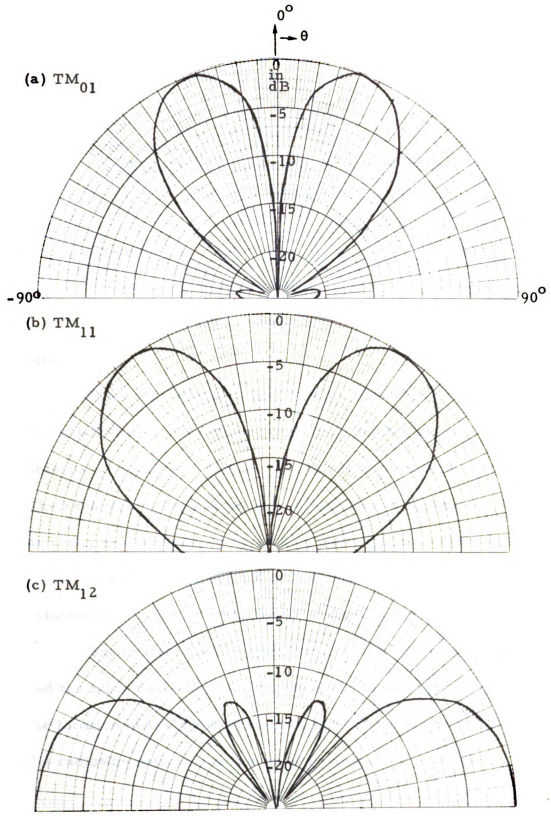

Fig. 2.6 Radiation patterns for (a) TM_{01} mode, (b) TM_{11} mode, (c) TM_{12} mode.

CHAPTER 3

OPEN-CAVITY RADIATORS WITH DIPOLE AND DIPOLE ARRAY EXCITERS

3.1 Introduction

In this chapter, the radiation and circuit properties of an open-cavity radiator with a dipole or a dipole array exciter are studied.

Since the expansion coefficients of waveguide modes are evaluated based on a given current distribution on the antenna, the antenna currents in a dipole and a dipole array are determined first. The zeroth-order currents for a dipole or for the dipole elements in an array are determined by solving Hallen's integral equations[11].

The total field excited in the cavity due to a dipole array is obtained by summing up the fields excited by each array element.

Theoretical and experimental results on the radiation pattern and the input resistance are obtained and compared. The effects of the location of the primary exciter and of rim length of the cavity on the radiation pattern and the input resistance are studied.

3.2 Expansion Coefficients and Input Resistance of the Radiator with a Dipole Exciter

3.2.1 Geometry and Trial Antenna Current

The geometry of the radiator with a dipole exciter is shown in Fig. 3.1. A thin dipole of length 2h is center-driven and located at the origin inside the open-cavity radiator. The current density on this dipole can be mathematically expressed as

$$\vec{J}_a(x, y, z) = \hat{y} \frac{I_o}{\sin\beta_o h} \delta(x)\delta(z)\sin\beta_o(h - |y|) \quad \text{for } -h \leq y \leq h \tag{3.1}$$

where I_o is the input current and β_o is the wave number in free-space. The circular cylinder is the same as that defined in Chapter 2. This cylinder is shorted at $z = -\ell_1$ and has an open end at $z = \ell_2$.

3.2.2 Expansion Coefficients

From Chapter 2, the expressions for the expansion coefficients for the qth waveguide mode in the open-cavity radiator are

$$B_q = \frac{\Gamma_{2q} M_q + N_q}{\Gamma_{1q}\Gamma_{2q} - 1}$$

$$C_q = \frac{\Gamma_{1q} N_q + M_q}{\Gamma_{1q}\Gamma_{2q} - 1}$$

where

$$M_q = \frac{\int_v \vec{E}_q^- \cdot \vec{J}_a \, dv}{2\int_{c.s.} (\vec{e}_q \times \vec{h}_q)\cdot \hat{z} \, ds}, \qquad N_q = \frac{\int_v \vec{E}_q^+ \cdot \vec{J}_a \, dv}{2\int_{c.s.} (\vec{e}_q \times \vec{h}_q)\cdot \hat{z} \, ds}$$

The numerators of M_q and N_q for the case of a dipole exciter can be found as

$$\int_v \vec{E}_q^- \cdot \vec{J}_a \, dv = \int_{c.s.} \int_{-\infty}^{\infty} (\vec{e}_q - \vec{e}_{zq}) e^{j\beta_q z} \cdot \vec{J}_a(x, y, z) \, dz \, ds$$

$$= \frac{I_o}{\sin \beta_o h} \int_{c.s.} \vec{e}_q \cdot \hat{y} \, \delta(x) \sin \beta_o (h - |y|) ds \qquad (3.2)$$

$$\int_v \vec{E}_q^+ \cdot \vec{J}_a \, dv = \int_{c.s.} \int_{-\infty}^{\infty} (\vec{e}_q + \vec{e}_{zq}) e^{-j\beta_q z} \cdot \vec{J}_a(x, y, z) dz \, ds$$

$$= \frac{I_o}{\sin \beta_o h} \int_{c.s.} \vec{e}_q \cdot \hat{y} \, \delta(x) \sin \beta_o (h - |y|) ds \qquad (3.3)$$

Since $(\vec{e}_q \times \vec{h}_q) \cdot \hat{z} = \vec{e}_q \times (\frac{1}{Z_q} \hat{z} \times \vec{e}_q) \cdot \hat{z} = \frac{1}{Z_q} (\vec{e}_q \cdot \vec{e}_q)$

therefore M_q and N_q become

$$M_q = N_q = \frac{I_o Z_q}{2 \sin \beta_o h} \frac{\int_{c.s.} \vec{e}_q \cdot \hat{y} \, \delta(x) \sin \beta_o (h - |y|) ds}{\int_{c.s.} (\vec{e}_q \cdot \vec{e}_q) ds} \qquad (3.4)$$

Let us define I_{Nq} and I_{Dq} as follows:

$$I_{Nq} = \int_{c.s.} \vec{e}_q \cdot \hat{y} \, \delta(x) \sin \beta_o (h - |y|) ds \qquad (3.5a)$$

$$I_{Dq} = \int_{c.s.} (\vec{e}_q \cdot \vec{e}_q) ds \qquad (3.5b)$$

The cylindrical coordinates (r, ϕ, z) and the rectangular coordinates (x, y, z) have relations of

$$\hat{y} = \hat{r} \sin\phi + \hat{\phi} \cos\phi$$

$$x = r \cos\phi, \quad y = r \sin\phi$$

Substituting the above relations into eq. (3.5a), we have

$$I_{Nq} = \int_0^h \int_{-\pi}^{\pi} \vec{e}_q(r, \phi) \cdot (\hat{r} \sin\phi + \hat{\phi} \cos\phi) \delta(r \cos\phi) \sin \beta_o (h - |r \sin\phi|) r \, d\phi \, dr$$

In the integration w.r.t. ϕ, $\delta(r\cos\phi)$ can be expressed as

$$\delta(r\cos\phi) = \frac{1}{r}\,\delta(\cos\phi) \tag{3.6}$$

Then

$$\begin{aligned} I_{Nq} &= \int_o^h \int_{-\pi}^{o} \vec{e}_q \cdot (\hat{r}\sin\phi + \hat{\phi}\cos\phi)\delta(\cos\phi)\sin\beta_o(h + r\sin\phi)\,d\phi\,dr \\ &\quad + \int_o^h \int_{o}^{\pi} \vec{e}_q \cdot (\hat{r}\sin\phi + \hat{\phi}\cos\phi)\delta(\cos\phi)\sin\beta_o(h - r\sin\phi)\,d\phi\,dr \\ &= \int_o^h [e_{rq}(\phi=\tfrac{\pi}{2}) - e_{rq}(\phi=-\tfrac{\pi}{2})]\sin\beta_o(h-r)dr \end{aligned} \tag{3.7}$$

where e_{rq} is the r-component of the electric field of the qth waveguide mode. I_{Dq} can be expressed as

$$I_{Dq} = \int_o^A \int_{-\pi}^{\pi} [(e_{rq})^2 + (e_{\phi q})^2]\, r\,d\phi\,dr \tag{3.8}$$

Therefore, the expansion coefficients B_q and C_q can be written as

$$B_q = \frac{I_o Z_q}{2\sin\beta_o h}\,\frac{I_{Nq}}{I_{Dq}}\,\frac{\Gamma_{2q}+1}{\Gamma_{1q}\Gamma_{2q}-1} \tag{3.9}$$

$$C_q = \frac{I_o Z_q}{2\sin\beta_o h}\,\frac{I_{Nq}}{I_{Dq}}\,\frac{\Gamma_{1q}+1}{\Gamma_{1q}\Gamma_{2q}-1} \tag{3.10}$$

Up to this point, the expansion coefficients are completely determined in terms of integrations w.r.t. r and ϕ. The determination of I_{Nq} and I_{Dq} for all the TE and TM modes can be made by substituting the mode field distributions into eqs. (3.7)and (3.8).

(i) TE Modes:

The transverse electric fields for the qth TE waveguide mode are

$$e_{rq} = \frac{n}{k_{cq}} \frac{J_n(k_{cq}r)}{r} \sin(n\phi) \tag{3.11a}$$

$$e_{\phi q} = J'_n(k_{cq}r)\cos(n\phi) \tag{3.11b}$$

Therefore I_{Nq} and I_{Dq} can be obtained as

$$I_{Nq} = \int_o^h \frac{n}{k_{cq}} \frac{J_n(k_{cq}r)}{r} [\sin(\frac{n\pi}{2}) - \sin(-\frac{n\pi}{2})] \sin\beta_o(h-r)dr$$

$$= \frac{2n\sin(\frac{n\pi}{2})}{k_{cq}} \int_o^h \frac{J_n(k_{cq}r)}{r} \sin\beta_o(h-r)dr \tag{3.12a}$$

and

$$I_{Dq} = \int_o^A \int_{-\pi}^{\pi} [\frac{n^2}{k_{cq}^2} \frac{J_n^2(k_{cq}r)}{r^2} \sin^2(n\phi) + J'^2_n(k_{cq}r)\cos^2(n\phi)] \, r \, d\phi \, dr$$

$$= \pi \int_o^A [\frac{n^2}{k_{cq}^2} \frac{J_n^2(k_{cq}r)}{r} + r J'^2_n(k_{cq}r)] dr \tag{3.12b}$$

(ii) TM Modes:

The transverse components of the electric field for the q th TM mode are

$$e_{rq} = J'_n(k_{cq}r)\sin(n\phi) \tag{3.13a}$$

$$e_{\phi q} = \frac{n}{k_{cq}} \frac{J_n(k_{cq}r)}{r} \cos(n\phi) \tag{3.13b}$$

so that

$$I_{Nq} = \int_o^h J'_n(k_{cq}r)[\sin(\frac{n\pi}{2}) - \sin(-\frac{n\pi}{2})] \sin\beta_o(h-r)dr$$

$$= 2\sin(\frac{n\pi}{2}) \int_o^h J'_n(k_{cq}r)\sin\beta_o(h-r)dr \tag{3.14a}$$

and

$$I_{Dq} = \pi \int_0^A \left[\frac{n^2}{k_{cq}^2} \frac{J_n^2(k_{cq}r)}{r} + r J_n'^2(k_{cq}r) \right] dr \qquad (3.14b)$$

The integrations for I_{Nq} and I_{Dq} are carried out numerically by a CDC 6500 computer.

3.2.3 Input Resistance

From Chapter 2, input resistance has been defined as

$$R_{in} = \frac{1}{I_o I_o^*} \sum_q \frac{|C_q|^2}{Z_q} (1 - |\Gamma_{2q}|^2) \int_{c.s.} \vec{e}_q \cdot \vec{e}_q \, ds \qquad (3.15)$$

Equation (3.15) is summing up only the propagating modes. Since the input current is real and I_{Dq} is defined in the previous section, eq. (3.15) can be rewritten as

$$R_{in} = \frac{1}{I_o^2} \sum_q \frac{|C_q|^2}{Z_q} (1 - |\Gamma_{2q}|^2) I_{Dq} \qquad (3.16)$$

3.3 Expansion Coefficients and Input Resistance of the Radiator with a Dipole Array Exciter

As the extension, an open-cavity radiator with a dipole array exciter will be considered in this section.

The currents in the driven element and the parasitic elements are determined first by solving Hallen's integral equations. The superposition principle is then employed to calculate the expansion coefficients due to individual antenna elements. After some phase

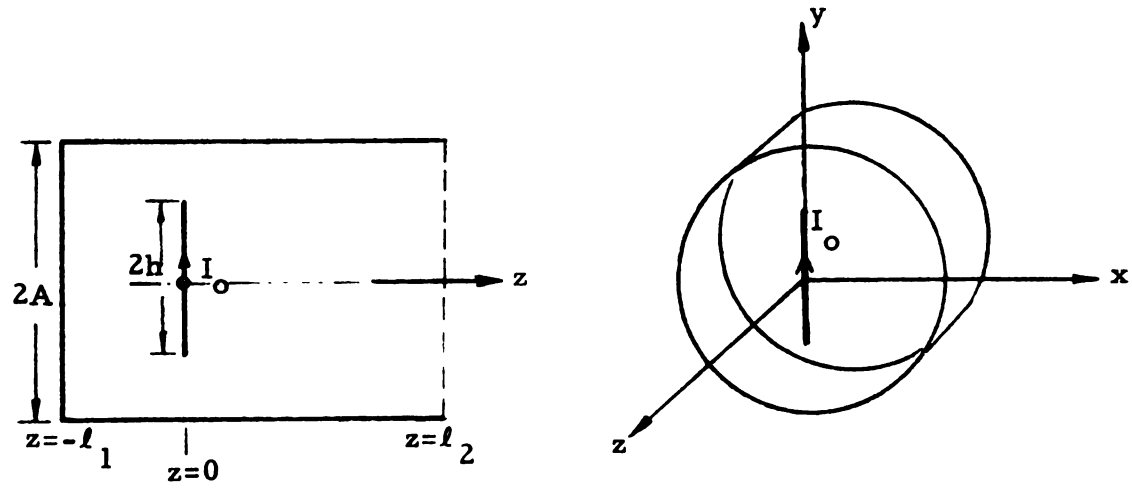

Fig. 3.1 Geometry of the radiator with a dipole exciter.

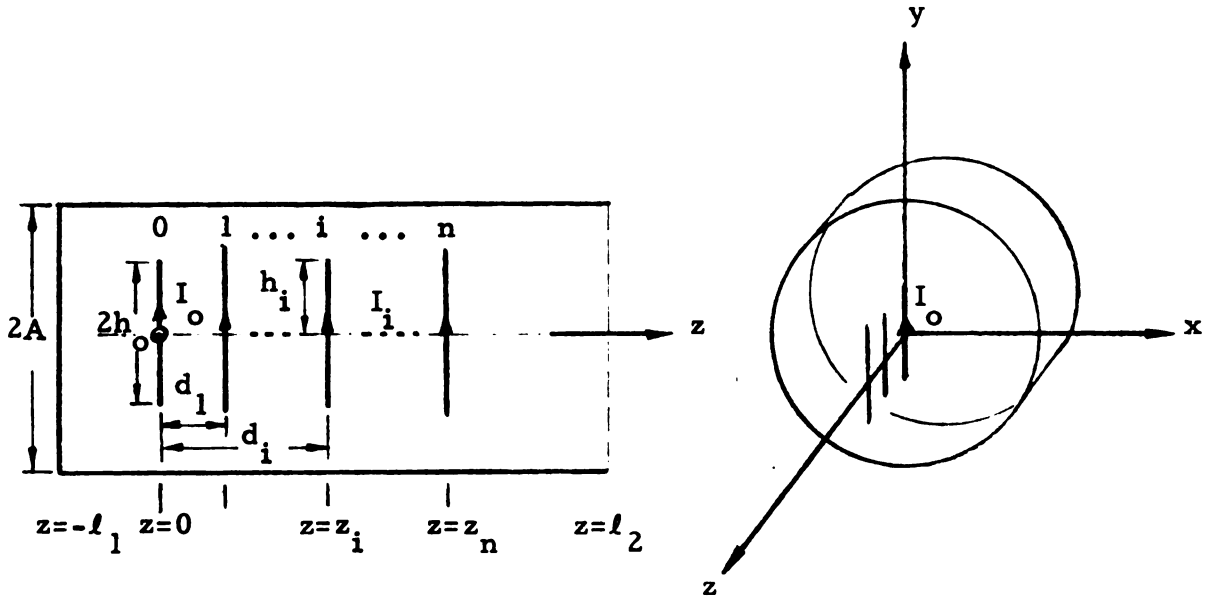

Fig. 3.2 Geometry of the radiator with a dipole array exciter.

modifications, those expansion coefficients are summed up to yield the total expansion coefficients which are then used to find the input resistance.

3.3.1 Geometry

Figure 3.2 shows a dipole array with n parasitic elements placed inside the circular cavity. The driven element is the zeroth element of the array and has a length of $2h_o$. The input current to this driven array dipole is I_o with a frequency of ω. The n parasitic elements are arranged along the z-axis and symmetric to the x-z plane. For the i th element, I_i, h_i and d_i are the input current, the antenna half-length and the distance between this element and the driven element, respectively. The input current I_i is obtained by solving the Hallen's integral equations[12] for the array and taking into account of a ground plane placed at a distance of ℓ_1 from the driven element.

3.3.2 Expansion Coefficients B_q and C_q

Let us define B_{iq} and C_{iq} as the expansion coefficients of the q th waveguide mode excited by i th parasitic element. B_q and C_q are the total expansion coefficients of the q th mode excited by all the elements of the dipole array. If we use a new coordinate system (x_i, y_i, z_i) with $x_i=x$, $y_i=y$ and $z=z_i+d_i$ for the i th element, we can find the B_{iq} and C_{iq} by the same procedure as for single dipole case as discussed in Section 3.2. The electric field due to the i th element, from eq. (2.4), is

$$\vec{E}_{il} = \sum_q B_{iq}[(\vec{e}_q - \vec{e}_{zq})e^{j\beta_q z_i} + \Gamma^i_{1q}(\vec{e}_q + \vec{e}_{zq})e^{-j\beta_q z_i}] \quad z_i < 0 \tag{3.17}$$

where Γ^i_{1q} is the reflection coefficient of the q th mode due to the short-circuit at $z_i = -(d_i + \ell_1)$. It follows that

$$\Gamma^i_{1q} = -e^{-j2\beta_q \ell_{1i}} = -e^{-j2\beta_q(d_i+\ell_1)} = \Gamma_{1q}e^{-j2\beta_q d_i} \tag{3.18}$$

By substituting eq. (3.18) and $z_i = z - d_i$ into eq. (3.17), we obtain

$$\vec{E}_{il} = \sum_q B_{iq}e^{-j\beta_q d_i}[(\vec{e}_q - \vec{e}_{zq})e^{j\beta_q z} + \Gamma_{1q}(\vec{e}_q + \vec{e}_{zq})e^{-j\beta_q z}] \tag{3.19}$$

Similary, E_{i2} is

$$\vec{E}_{i2} = \sum_q C_{iq}e^{j\beta_q d_i}[(\vec{e}_q + \vec{e}_{zq})e^{-j\beta_q z} + \Gamma_{2q}(\vec{e}_q - \vec{e}_{zq})e^{j\beta_q z}] \tag{3.20}$$

Summing up all the fields due to all the dipole elements, the total $\vec{E}$ field in the waveguide is

$$\vec{E}_1 = \sum_{i=0}^{n} \sum_q B_{1q}e^{-j\beta_q d_i}[(\vec{e}_q - \vec{e}_{zq})e^{j\beta_q z} + \Gamma_{1q}(\vec{e}_q + \vec{e}_{zq})e^{-j\beta_q z}]$$

$$= \sum_q B_q[(\vec{e}_q - \vec{e}_{zq})e^{j\beta_q z} + \Gamma_{1q}(\vec{e}_q + \vec{e}_{zq})e^{-j\beta_q z}] \tag{3.21a}$$

and $$\vec{E}_2 = \sum_q C_q[(\vec{e}_q + \vec{e}_{zq})e^{-j\beta_q z} + \Gamma_{2q}(\vec{e}_q - \vec{e}_{zq})e^{j\beta_q z}] \tag{3.21b}$$

where $$B_q = \sum_{i=0}^{n} B_{iq}e^{-j\beta_q d_i} \tag{3.22a}$$

and $$C_q = \sum_{i=0}^{n} C_{iq}e^{j\beta_q d_i} \tag{3.22b}$$

are the total expansion coefficients for the q th mode excited by the

dipole array. It is noted that d_o in eqs. (3.22) is zero.

3.3.3 Input Resistance

Equation (3.16) is also valid for the dipole array case except that C_q is the total expansion coefficient which has been found in eq. (3.22b). I_{Nq} remains the same as the case of a single dipole because the field distributions of the q th modes excited by all the array elements are assumed to be the same.

3.4 Experimental Setup

The experimental setup for the measurement of the radiation patterns and the input impedance of an open-cavity radiator is schematically shown in Fig. 3.3. The open-cavity radiator is placed inside an anechoic chamber, which is covered by microwave absorbers. The radius A of the cylindrical cavity is 10 cm and is equal to one free-space wavelength under the operating frequency. The rim length $\ell_1 + \ell_2$ of the radiator is made adjustable for the experimental purposes. A movable receiving antenna is used to measure the radiation patterns of the radiator. The distance between the radiator and the receiving antenna is 50 cm (5 λ_o) when the rim length is adjusted to be 10 cm. By rotating the position of the radiator, this receiving antenna can measure both the E-plane and H-plane radiation patterns.

The primary radiator, namely, the dipole exciter or the dipole array excier, is excited by an R.F. oscillator at 3 GHz and

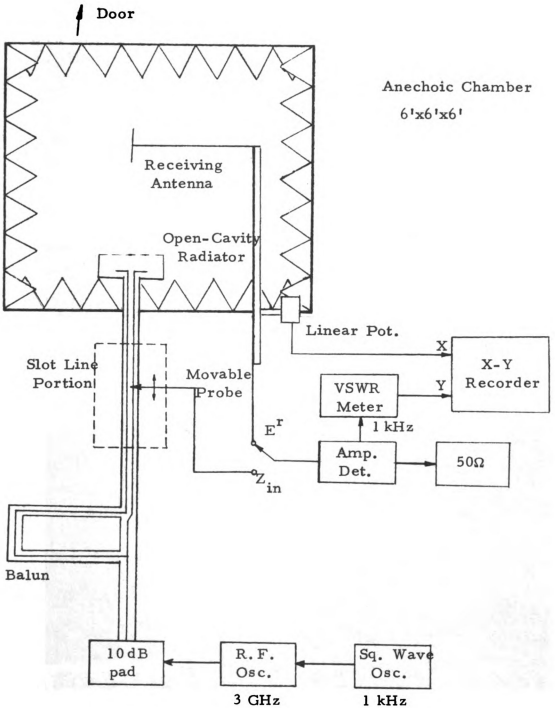

Fig. 3.3 Experimental setup for the open-cavity radiator.

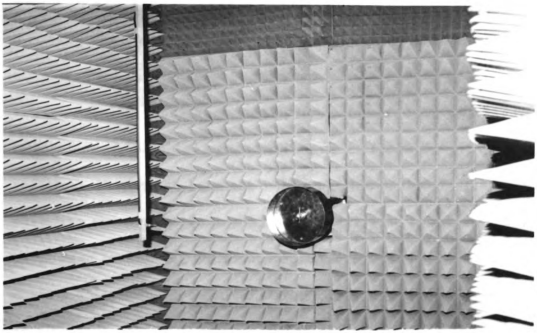

Fig. 3.4 Open-cavity radiator with a dipole exciter inside the anechoic chamber.

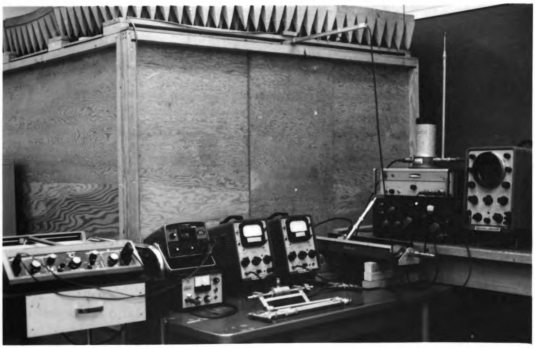

Fig. 3.5 The experimental setup outside the anechoic chamber.

with a square wave amplitude modulation of 1 KHz. Fig. 3.4 shows a receiving antenna and an open-cavity radiator with a dipole exciter all placed inside an anechoic chamber.

A balun[13] has been employed to convert a GR coaxial line to a balanced, shielded two-wire line which feeds the primary radiator. A slot has been cut over a portion of the shielded two-wire line and a movable probe has been inserted in the slot, for the purpose of measuring the input impedance of the primary radiator. A simple detecting system consisting of an amplitude detector and an SWR indicator has been used to measure both the radiation field and the input impedance. An x-y recorder has been used to obtain a direct plot of the radiation patterns. Fig. 3.5 is a photograph showing the experiment setup outside the anechoic chamber.

3.5 Comparison between Theory and Experiment

Theoretical and experimental results on the radiation patterns and the input resistance of an open-cavity radiator with a dipole or a dipole array exciter are obtained and compared in this section.

In the theoretical calculation for the radiation patterns and the input resistance, all the propagating TE and TM waveguide modes are considered. Some of the cutoff modes have also been considered in addition to the propagating modes to see their effect on radiation patterns. The effect was found to be insignificant

when the total rim length was over $0.6\lambda_o$. The theoretical results on the radiation patterns and the input resistance are calculated numerically by a CDC 6500 computer.

Figures 3.6 to 3.17 show the E-plane ($\phi=90^o$) and H-plane ($\phi=0^o$) radiation patterns of open-cavity radiators with various dimensions, different locations of primary exciters, and various rim lengths of the cavity. The theoretical results (dotted line) and experimental results (solid line) are plotted together for easy comparison. In all these figures, a satisfactory agreement between theory and experiment is observed.

Figures 3.6 to 3.8 show the radiation patterns of an open-cavity radiator with a dipole exciter and a variable rim length. The dipole exciter with a half length of $\lambda_o/4$ is located $\lambda_o/4$ away from the shorted end. The rim lengths of cavity for these three figures are $0.8\lambda_o$, $1.0\lambda_o$ and $1.2\lambda_o$ respectively. The effect of the cavity length on the H-plane pattern is found to be rather significant. Figures 3.9 to 3.11 give the radiation patterns of open-cavity radiators with three different dipole exciters placed at the same position as the first three figures and with the rim length fixed at $1.0\lambda_o$. The dipole half lengths for these three figures are $0.05\lambda_o$, $0.15\lambda_o$ to $0.35\lambda_o$. The effect of the dipole length on the radiation pattern is not very significant. Figures 3.12 to 3.14 illustrate the radiation patterns of the radiators with a dipole exciter placed at three different distances, $0.15\lambda_o$, $0.1\lambda_o$ and $0.05\lambda_o$ from the

shorted end of the cavity. The rim length is kept at $1.0\lambda_o$ for these three cases. The effect of the exciter location on the radiation pattern is found to be insignificant.

Figures 3.15 to 3.17 show the radiation patterns of an open-cavity radiator with a two-element dipole array primary exciter for three different rim lengths. The driven element with a half-length of $\lambda_o/4$ is placed $\lambda_o/4$ away from the shorted end of the cavity. The parasitic element has a half length of $0.22\lambda_o$ and is located $0.25\lambda_o$ from the driven element. The three different rim lengths are $0.8\lambda_o$, $1.0\lambda_o$ and $1.2\lambda_o$ respectively. It is observed that the H-plane pattern is greatly improved with a dipole array exciter compared with the case of a dipole exciter.

The experimental result of input resistance of an open-cavity radiator is compared with the theoretical input resistance, while the experimental reactance is not checked due to lack of theoretical reactance. Table 3.1 shows the comparison between experimental and theoretical resistances of an open-cavity radiator with a dipole exciter which has a half length of $0.25\lambda_o$ and placed at a distance of $0.25\lambda_o$ from shorted end of the cavity. The rim length is varied from $0.6\lambda_o$ to $1.2\lambda_o$. Table 3.2 shows the same comparison as Table 3.1 for a same radiator with a dipole exciter of a $0.32\lambda_o$ half length. Table 3.3 shows the theoretical and experimental input resistances of a same radiator with a dipole array exciter with dimensions described in Fig. 3.15 to Fig. 3.17.

Table 3.1 Experimental Input Impedance and Theoretical Input Resistance of an Open-Cavity Radiator with a Dipole Exciter $h = 0.25\lambda_o$, $\ell_1 = 0.25\lambda_o$.

Rim Length $L = \ell_1 + \ell_2$	Experimental Input Impedance	Theoretical Input Resistance
$0.6\lambda_o$	86.5 + j19.5	60.97
$0.8\lambda_o$	71.1 + j82.4	67.69
$1.0\lambda_o$	78.7 + j53.4	70.73
$1.2\lambda_o$	89.6 + j86.3	70.99

Table 3.2 Experimental Input Impedance and Theoretical Input Resistance of an Open Cavity Radiator with a Dipole Exciter $h = 0.32\lambda_o$, $\ell_1 = 0.25\lambda_o$.

Rim Length $L = \ell_1 + \ell_2$	Experimental Input Impedance	Theoretical Input Resistance
$0.6\lambda_o$	153.8 + j163.8	188.12
$0.8\lambda_o$	148.5 + j165.2	208.10
$1.0\lambda_o$	175.2 + j199.5	217.76
$1.2\lambda_o$	146.2 + j172.8	218.5

Table 3.3 Experimental Input Impedance and Theoretical Input Resistance of an Open-Cavity Radiator with a Dipole Array Exciter $h_o = 0.25\lambda_o$, $h_1 = 0.22\lambda_o$, $\ell_1 = 0.25\lambda_o$ and $d_1 = 0.25\lambda_o$.

Rim Length $L = \ell_1 + \ell_2$	Experimental Input Impedance	Theoretical Input Resistance
$0.8\lambda_o$	52.1 + j118.2	56.6
$1.0\lambda_o$	68.6 + j71.2	60.6
$1.2\lambda_o$	57.6 + j121.9	49.3

In these three tables, a qualitative agreement is obtained between theory and experiment.

3.6 Conclusion

A theoretical analysis on the radiation and circuit properties of an open-cavity radiator with a dipole or a dipole array exciter has been carried out in this chapter. Theoretical results have been confirmed by experimental results.

Concerning the radiation patterns, a few points of interest are as follows: (a) The radiation patterns of a radiator are quite independent of the length and the location of the dipole exciter. This implies that a proper exciter may be chosen to improve the matching with the driving line while keeping the desired radiation patterns unchanged. (b) The rim length of the cavity has a rather significant effect on the H-plane pattern. (c) A radiator with a two-element dipole array exciter gives very desirable radiation patterns both in the E-plane and the H-plane. No side lobes appear in the patterns. A radiator with this exciter may prove to function better than usual backfire antenna with a dipole exciter and a small reflecting plate.

Among these figures on the radiation patterns, rather large disagreements between theory and experiment are recorded in some cases. The sources of discrepancy are believed to be due to: (a) negligence of the diffraction at the radiator aperture, (b) inaccurate calculation of the reflection of the propagating modes at the aperture,

and (c) the effect of the cut-off mode fields specially for the cases of short cavity rims.

For the input impedance of the open-cavity radiator, the present analysis yields only the theoretical input resistance which is in qualitative agreement with the experimental results. Generally speaking the input impedance is not strongly dependent on the cavity dimensions.

From the results presented in this chapter, it is concluded that the radiation property of the open-cavity radiator is essentially controlled by the cavity dimensions while the circuit property of the radiator is primarily determined by the geometry of the exciter. These characteristics may lead to the advantages of separate controls of the radiation and circuit properties and, therefore, an easier design of an open-cavity radiator.

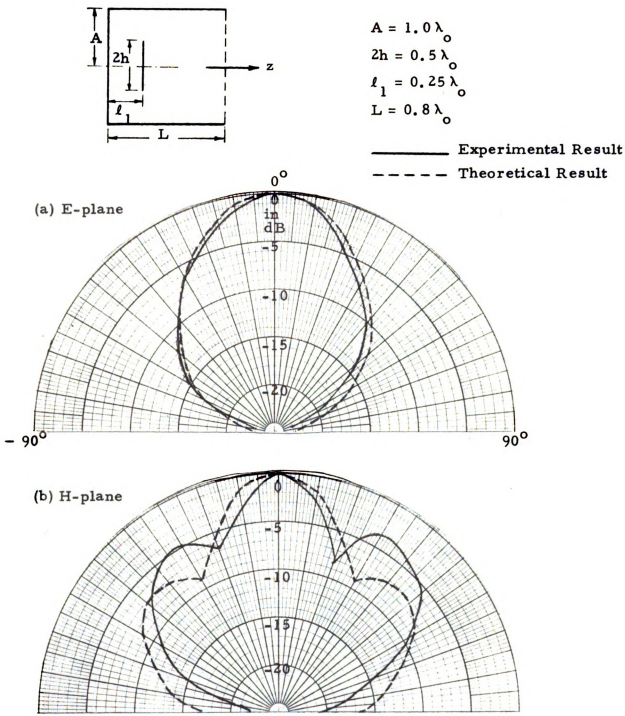

Fig. 3.6 Radiation patterns of an open-cavity radiator with a dipole exciter (h = 0.25 λ_o, ℓ_1 = 0.25 λ_o, L = 0.8 λ_o).

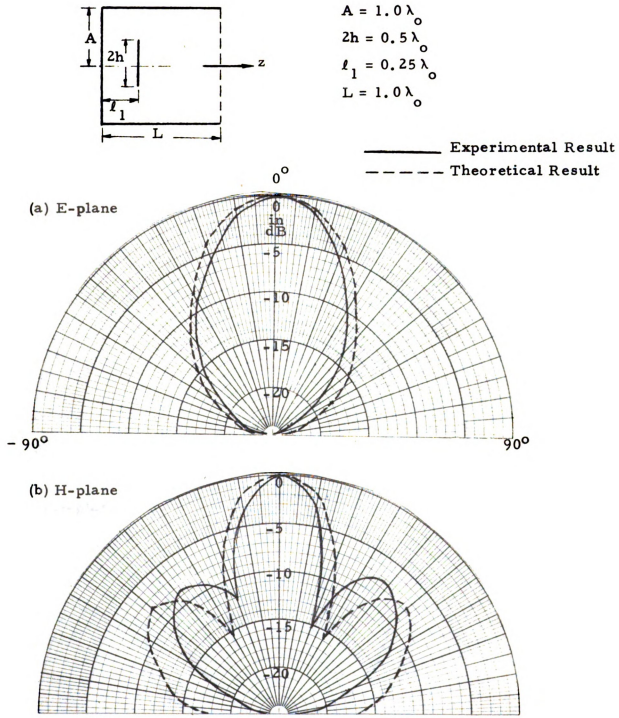

Fig. 3.7 Radiation patterns of an open-cavity radiator with a dipole exciter (h = 0.25 λ_o, ℓ_1 = 0.25 λ_o, L = 1.0 λ_o).

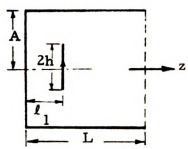

$A = 1.0\ \lambda_o$
$2h = 0.5\ \lambda_o$
$\ell_1 = 0.25\ \lambda_o$
$L = 1.2\ \lambda_o$

Experimental Result
Theoretical Result

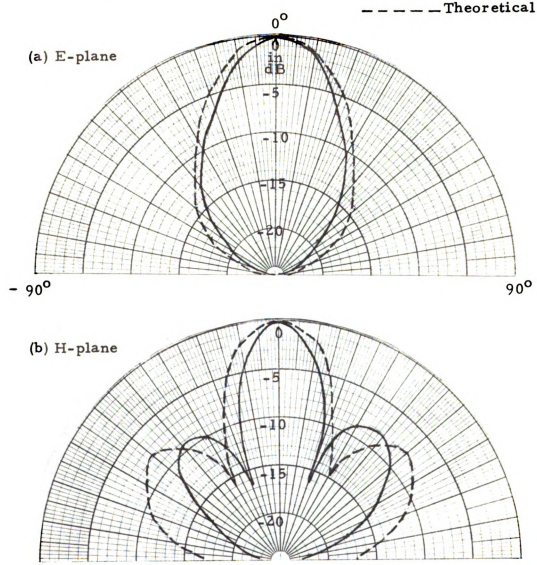

Fig. 3.8 Radiation patterns of an open-cavity radiator with a dipole exciter ($h = 0.25\ \lambda_o$, $\ell_1 = 0.25\ \lambda_o$, $L = 1.2\ \lambda_o$).

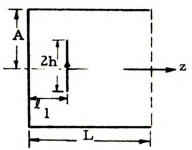

$A = 1.0\ \lambda_o$
$2h = 0.10\ \lambda_o$
$\ell_1 = 0.25\ \lambda_o$
$L = 1.0\ \lambda_o$

Experimental Result
Theoretical Result

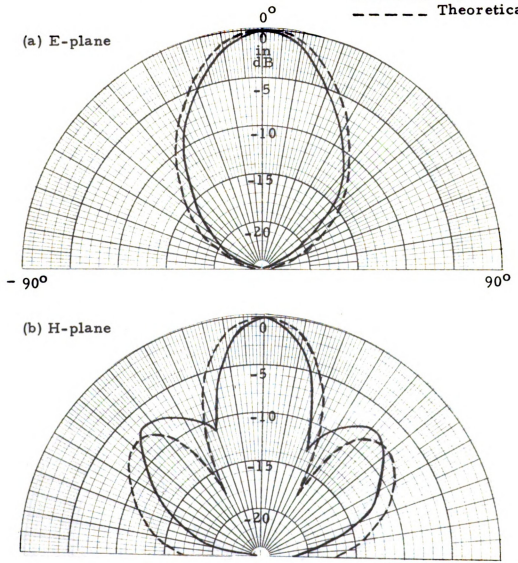

Fig. 3.9 Radiation patterns of an open-cavity radiator with a dipole exciter ($h = 0.05\ \lambda_o$, $\ell_1 = 0.25\ \lambda_o$, $L = 1.0\ \lambda_o$).

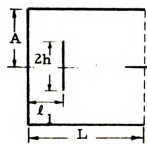

$A = 1.0\ \lambda_o$
$2h = 0.30\ \lambda_o$
$\ell_1 = 0.25\ \lambda_o$
$L = 1.0\ \lambda_o$

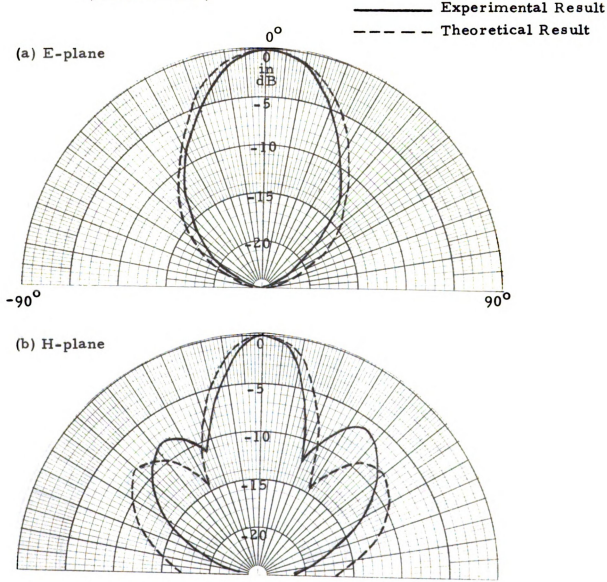

Fig. 3.10 Radiation patterns of an open-cavity radiator with a dipole exciter ($h = 0.15$, $\ell_1 = 0.25\ \lambda_o$, $L = 1.0\ \lambda_o$).

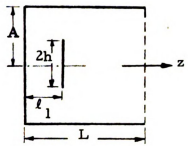

A = 1.0 λ_o
2h = 0.70 λ_o
ℓ_1 = 0.25 λ_o
L = 1.0 λ_o

Experimental Result
Theoretical Result

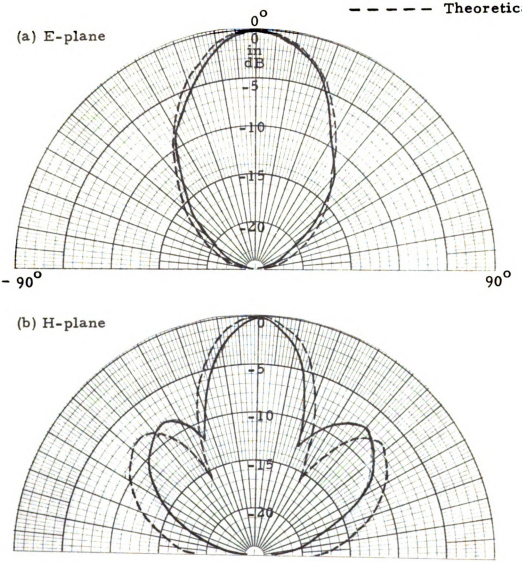

Fig. 3.11 Radiation patterns of an open-cavity radiator with a dipole exciter (h = 0.35 λ_o, ℓ_1 = 0.25 λ_o, L = 1.0 λ_o).

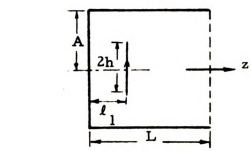

$A = 1.0\,\lambda_o$
$2h = 0.50\,\lambda_o$
$\ell_1 = 0.15\,\lambda_o$
$L = 1.0\,\lambda_o$

Experimental Result
Theoretical Result

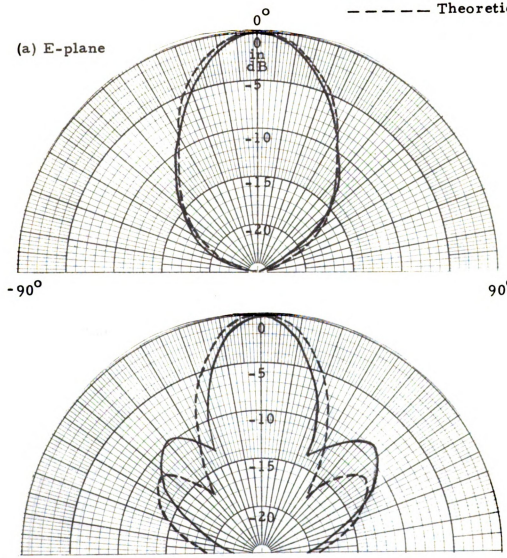

Fig. 3.12 Radiation patterns of an open-cavity radiator with a dipole exciter ($h = 0.25\,\lambda_o$, $\ell_1 = 0.15\lambda_o$, $L = 1.0\,\lambda_o$).

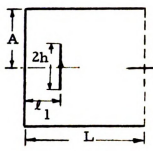

$A = 1.0\ \lambda_o$
$2h = 0.50\ \lambda_o$
$\ell_1 = 0.10\ \lambda_o$
$L = 1.0\ \lambda_o$

Experimental Result
Theoretical Result

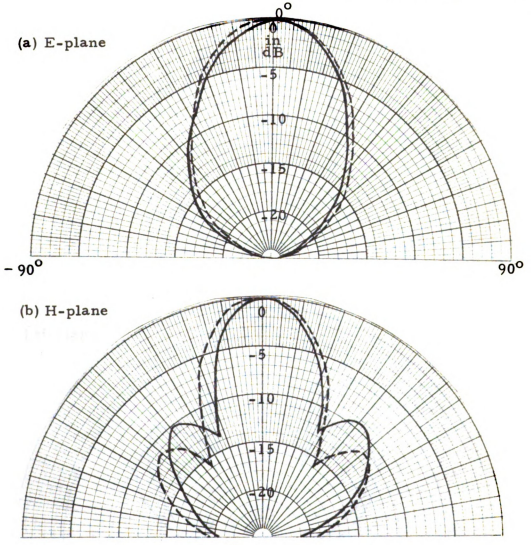

Fig. 3.13 Radiation patterns of an open-cavity radiator with a dipole exciter ($h = 0.25\ \lambda_o$, $\ell_1 = 0.10\ \lambda_o$, $L = 1.0\ \lambda_o$).

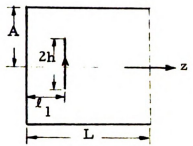

$A = 1.0\ \lambda_o$

$2h = 0.50\ \lambda_o$

$\ell_1 = 0.05\ \lambda_o$

$L = 1.0\ \lambda_o$

Experimental Result

Theoretical Result

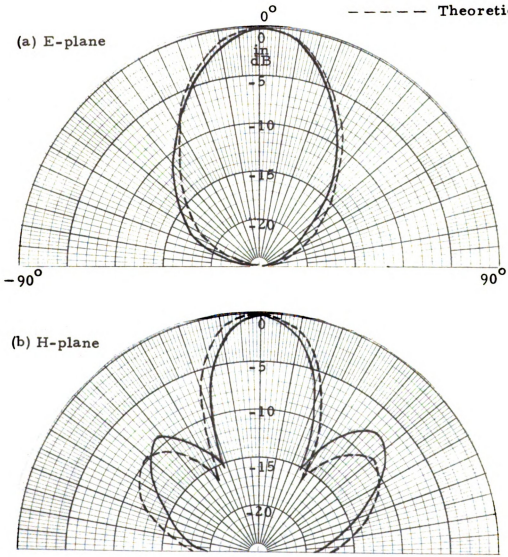

Fig. 3.14 Radiation patterns of an open-cavity radiator with a dipole exciter ($h = 0.25\ \lambda_o$, $\ell_1 = 0.05\ \lambda_o$, $L = 1.0\ \lambda_o$).

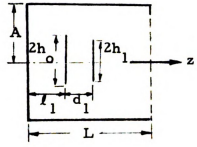

$A = 1.0\ \lambda_o$

$2h_o = 0.5\ \lambda_o$, $2h_p = 0.22\ \lambda_o$

$\ell_1 = 0.25\ \lambda_o$, $d_1 = 0.25\ \lambda_o$

$L = 0.8\ \lambda_o$

Experimental Result

Theoretical Result

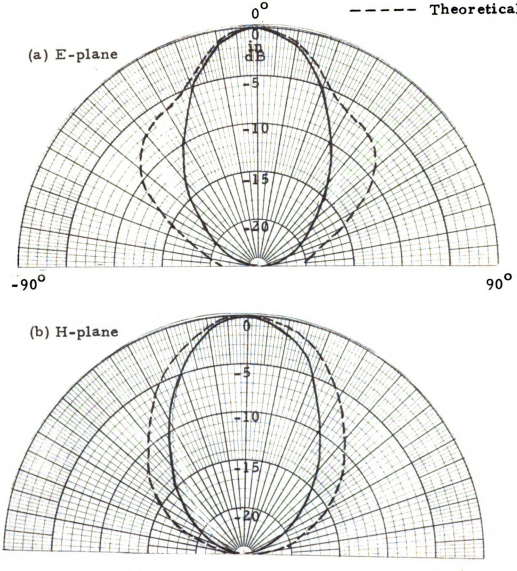

Fig. 3.15 Radiation patterns of an open-cavity radiator with a dipole array exciter ($h_o = 0.25\lambda_o$, $h_1 = 0.22\lambda_o$, $\ell_1 = 0.25\lambda_o$, $d_1 = 0.25\lambda_o$, $L = 0.8\lambda_o$).

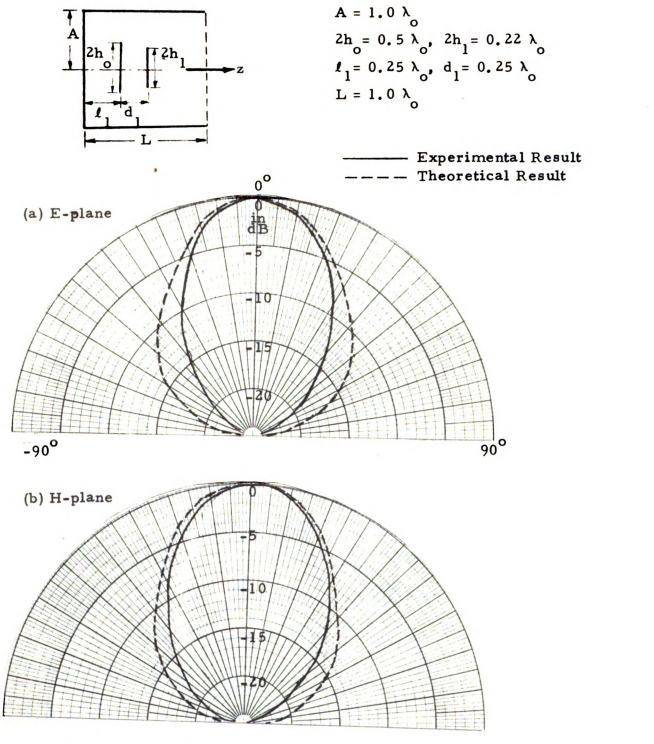

Fig. 3.16 Radiation patterns of an open-cavity radiator with a dipole array exciter ($h_o = 0.25\ \lambda_o$, $h_1 = 0.22\ \lambda_o$, $\ell_1 = 0.25\ \lambda_o$, $d_1 = 0.25\ \lambda_o$, $L = 1.0\ \lambda_o$).

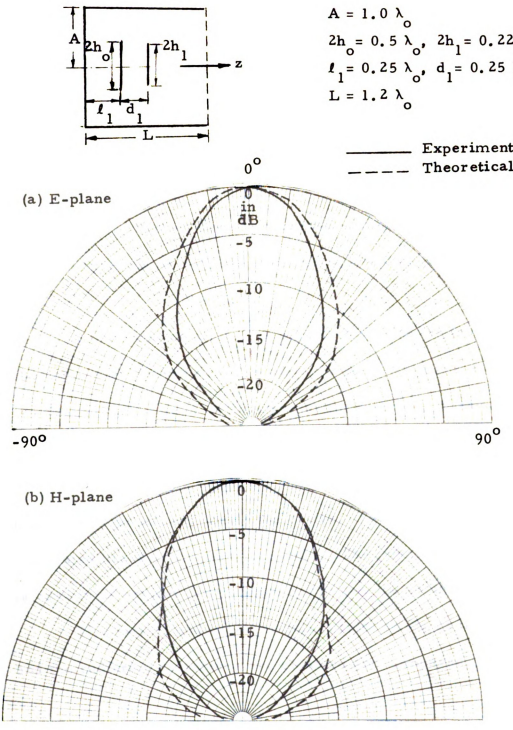

Fig. 3.17 Radiation patterns of an open-cavity radiator with a dipole array exciter ($h_o = 0.25\ \lambda_o$, $h_1 = 0.22\ \lambda_o$, $\ell_1 = 0.25\ \lambda_o$, $d_1 = 0.25\ \lambda_o$, $L = 1.2\ \lambda_o$).

CHAPTER 4

OPEN-CAVITY RADIATORS WITH TRANSMISSION LINE EXCITERS

4.1 Introduction

In this chapter, the radiation and circuit properties of an open-cavity radiator with a transmission line type exciter are studied.

A thin conducting wire is placed closely in the front of the shorted end of the cavity. The wire and its image form a section of a transmission line. With a proper termination, a traveling wave of current can be excited on the transmission line.

The waveguide excitation theory has been employed to determine the fields excited inside the cavity. The radiation fields are calculated based on the aperture field. The Poynting vector method is used to determine the radiated power and the radiation resistance.

Theoretical and experimental results on the radiation patterns and the radiation resistance are obtained and compared.

4.2 Expansion Coefficients and Radiation Resistance of an Open-Cavity Radiator with a Transmission Line Exciter

4.2.1 Geometry

The geometry of an open-cavity radiator with a transmission line exciter is shown in Fig. 4.1. A section of thin conducting wire with a length of 2h is located on y-z plane. The total current flowing in the wire is I_o and the frequency is ω. If the spacing between the conducting wire and the shorted end, ℓ_1, is small, the conducting wire and its image form a section of a transmission line with a characteristic impedance of Z_c. If this section of transmission line is terminated with a resistor of $Z^t = Z_c/2$, a traveling wave of current can be excited in the wire. Mathematically, this current can be represented by a current density $\vec{J}_a$ such as,

$$\vec{J}_a(x, y, z) = \hat{y}\, I_o \delta(z)\delta(x)\, e^{-j\beta_o(y+h)} \quad \text{for } -h \leq y \leq h \qquad (4.1)$$

where I_o is the input current at y = -h, and β_o is the wave number in the free-space. The two short ends of the transmission line will be ignored in the theoretical analysis. The circular cylindrical cavity is the same as that defined in the previous chapter.

4.2.2 Expansion Coefficients

The expressions for the expansion coefficients for the q th mode excited in the open-cavity radiator have been given in Chapter 2 as,

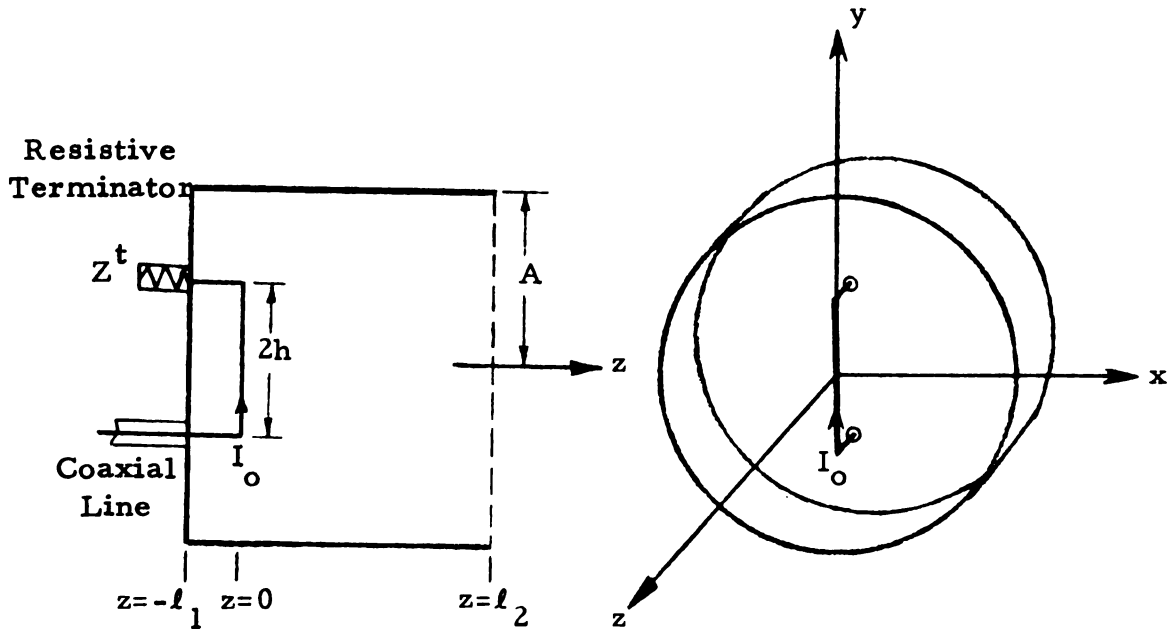

(a)

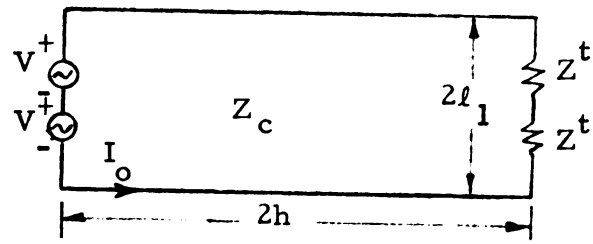

(b)

Fig. 4.1 Geometry of an open-cavity radiator with a transmission line exciter and the equivalent circuit of the transmission line exciter.

$$B_q = \frac{\Gamma_{2q} M_q + N_q}{\Gamma_{1q}\Gamma_{2q} - 1}$$

$$C_q = \frac{\Gamma_{1q} N_q + M_q}{\Gamma_{1q}\Gamma_{2q} - 1}$$

where $M_q = \dfrac{\int_v \vec{E}_q^- \cdot \vec{J}_a \, dv}{2\int_{c.s.} (\vec{e}_q \times \vec{h}_q) \cdot \hat{z} \, ds}$, $N_q = \dfrac{\int_v \vec{E}_q^+ \cdot \vec{J}_a \, dv}{2\int_{c.s.} (\vec{e}_q \times \vec{h}_q) \cdot \hat{z} \, ds}$

The numerators of M_q and N_q for the case of a transmission line exciter can be found to be

$$\int_v \vec{E}_q^- \cdot \vec{J}_a dv = \int_{c.s.} \int_{\ell_1}^{\ell_2} (\vec{e}_q - \vec{e}_{zq}) e^{j\beta_q z} \cdot \hat{y} I_o \delta(z)\delta(x) e^{-j\beta_o (y+h)} \, dz \, ds$$

$$= I_o \int_{c.s.} \vec{e}_q \cdot \hat{y} \, \delta(x) e^{-j\beta_o (y+h)} \, ds \qquad (4.2)$$

and

$$\int_v \vec{E}_q^+ \cdot \vec{J}_a dv = I_o \int_{c.s.} \vec{e}_q \cdot \hat{y} \, \delta(x) e^{-j\beta_o (y+h)} \, ds = \int_v \vec{E}_q^- \cdot \vec{J}_a dv \qquad (4.3)$$

where $\int_{c.s.} ds$ is the surface integration over the cross-section of the waveguide. Since $(\vec{e}_q \times \vec{h}_q) \cdot \hat{z} = \frac{1}{Z_q} (\vec{e}_q \cdot \vec{e}_q)$, M_q and N_q can be expressed as

$$M_q = N_q = \frac{I_o Z_q}{2} \frac{\int_{c.s.} \vec{e}_q \cdot \hat{y} \, \delta(x) e^{-j\beta_o (y+h)} \, ds}{\int_{c.s.} (\vec{e}_q \cdot \vec{e}_q) ds} \qquad (4.4)$$

We define I_{Nq} and I_{Dq} as follows:

$$I_{Nq} = \int_{c.s.} \vec{e}_q \cdot \hat{y}\, \delta(x)\, e^{-j\beta_o(y+h)}\, ds \tag{4.5a}$$

$$I_{Dq} = \int_{c.s.} (\vec{e}_q \cdot \vec{e}_q) ds \tag{4.5b}$$

Converting to cylindrical coordinates, eq. (4.5a) becomes

$$I_{Nq} = \int_0^h \int_{-\pi}^{\pi} \vec{e}_q(r,\phi) \cdot (\hat{r}\sin\phi + \hat{\phi}\cos\phi)\delta(r\cos\phi)\, e^{-j\beta_o(r\sin\phi + h)}\, r\, d\phi dr$$

$$= \int_0^h \int_{-\pi}^{0} \vec{e}_q \cdot (\hat{r}\sin\phi + \hat{\phi}\cos\phi)\delta(r\cos\phi)\, e^{-j\beta_o(r\sin\phi + h)}\, r d\phi dr$$

$$+ \int_0^h \int_{0}^{\pi} \vec{e}_q \cdot (\hat{r}\sin\phi + \hat{\phi}\cos\phi)\delta(r\cos\phi)\, e^{-j\beta_o(r\sin\phi + h)}\, r d\phi dr$$

or

$$I_{Nq} = e^{-j\beta_o h} \int_0^h \left[e_{rq} e^{-j\beta_o r\sin\phi}\Big|_{\phi=\frac{\pi}{2}} - e_{rq} e^{-j\beta_o r\sin\phi}\Big|_{\phi=-\frac{\pi}{2}} \right] dr \tag{4.6}$$

and

$$I_{Dq} = \int_0^A \int_{-\pi}^{\pi} \left[(e_{rq})^2 + (e_{\phi q})^2 \right] r\, d\phi\, dr \tag{4.7}$$

where e_{rq} and $e_{\phi q}$ are the r and ϕ-components of the electric field of the qth waveguide mode.

Substituting the waveguide fields, e_{rq} and $e_{\phi q}$, into eqs. (4.6) and (4.7), I_{Nq} and I_{Dq} can be evaluated and the expansion coefficients for the qth mode are obtained as

$$B_q = \frac{Z_q I_o}{2} \frac{I_{Nq}}{I_{Dq}} \frac{\Gamma_{2q} + 1}{\Gamma_{1q}\Gamma_{2q} - 1} \tag{4.8}$$

$$C_q = \frac{Z_q I_o}{2} \frac{I_{Nq}}{I_{Dq}} \frac{\Gamma_{1q}+1}{\Gamma_{1q}\Gamma_{2q}-1} \tag{4.9}$$

The results of I_{Nq} and I_{Dq} for all the TE and TM modes are given as follows,

(i) TE Modes:

From Appendix, the transverse components of the electric field of the q th TE waveguide mode are

$$e_{rq} = \frac{n}{k_{cq}} \frac{J_n(k_{cq}r)}{r} \begin{cases} \sin(n\phi) \\ -\cos(n\phi) \end{cases}$$

$$e_{\phi q} = J'_n(k_{cq}r) \begin{cases} \cos(n\phi) \\ \sin(n\phi) \end{cases}$$

Therefore, I_{Nq} and I_{Dq} can be obtained as

$$I_{Nq} = e^{-j\beta_o h} \int_o^h \frac{n}{k_{cq}r} J_n(k_{cq}r)[e^{-j\beta_o r} \begin{cases} \sin\frac{n\pi}{2} \\ -\cos\frac{n\pi}{2} \end{cases} + e^{j\beta_o r} \begin{cases} \sin\frac{n\pi}{2} \\ \cos\frac{n\pi}{2} \end{cases}] dr$$

$$= 2e^{-j\beta_o h} \int_o^h \frac{n J_n(k_{cq}r)}{k_{cq}r} \begin{cases} \sin\frac{n\pi}{2}\cos\beta_o r \\ j\cos\frac{n\pi}{2}\sin\beta_o r \end{cases} dr \tag{4.10}$$

$$I_{Dq} = \pi \int_o^A [\frac{h^2}{k_{cq}^2} \frac{J_n^2(k_{cq}r)}{r} + r J'^2_n(k_{cq}r)] dr \tag{4.11}$$

In eq. (4.10), we choose the proper waveguide field expression which gives non-zero value of I_{Nq}. The n in eqs. (4.10) and (4.11) is positive integer, and when

(a) n is odd

$$I_{Nq} = \frac{2n}{k_{cq}} \sin\left(\frac{n\pi}{2}\right) e^{-j\beta_o h} \int_o^h \frac{J_n(k_{cq} r)\cos\beta_o r}{r}\, dr \qquad (4.12a)$$

$$e_{rq} = \frac{n}{k_{cq}} \frac{J_n(k_{cq} r)}{r} \sin n\phi \qquad (4.12b)$$

$$e_{\phi q} = J_n'(k_{cq} r) \cos n\phi \qquad (4.12c)$$

(b) n is even

$$I_{Nq} = j \frac{2n}{k_{cq}} \cos\left(\frac{n\pi}{2}\right) e^{-j\beta_o h} \int_o^h \frac{J_n(k_{cq} r)\sin\beta_o r}{r}\, dr \qquad (4.13a)$$

$$e_{rq} = -\frac{n}{k_{cq}} \frac{J_n(k_{cq} r)}{r} \cos n\phi \qquad (4.13b)$$

$$e_{\phi q} = J_n'(k_{cq} r) \sin n\phi \qquad (4.13c)$$

I_{Dq} is given in eq. (4.11)

(ii) TM Modes:

The transverse components of the electric field of the q th TM mode are

$$e_{rq} = J_n'(k_{cq} r) \begin{cases} \cos n\phi \\ \sin n\phi \end{cases}$$

$$e_{\phi q} = \frac{n}{k_{cq}} \frac{J_n(k_{cq} r)}{r} \begin{cases} -\sin n\phi \\ \cos n\phi \end{cases}$$

and

$$I_{Nq} = e^{-j\beta_o h} \int_o^h J'_n(k_{cq}r)\left[e^{-j\beta_o r}\begin{cases}\cos\frac{n\pi}{2}\\ \sin\frac{n\pi}{2}\end{cases} - e^{j\beta_o r}\begin{cases}\cos\frac{n\pi}{2}\\ -\sin\frac{n\pi}{2}\end{cases}\right] dr$$

$$= 2\, e^{-j\beta_o h} \int_o^h J'_n(k_{cq}r)\begin{cases}-j\sin\beta_o r\cos\frac{n\pi}{2}\\ \cos\beta_o r\sin\frac{n\pi}{2}\end{cases} dr \qquad (4.14)$$

$$I_{Dq} = \pi \int_o^A \left[\frac{n^2}{k_{cq}^2}\ \frac{J_n^2(k_{cq}r)}{r} + r\, J'^2_n(k_{cq}r)\right] dr \qquad (4.15)$$

Choosing the proper set of I_{Nq} and I_{Dq}, we have for

(a) n is odd

$$I_{Nq} = 2\sin\frac{n\pi}{2}\, e^{-j\beta_o h} \int_o^h J'_n(k_{cq}r)\cos\beta_o r\, dr \qquad (4.16a)$$

$$e_{rq} = J'_n(k_{cq}r)\sin n\phi \qquad (4.16b)$$

$$e_{\phi q} = \frac{n}{k_{cq}}\ \frac{J_n(k_{cq}r)}{r}\cos n\phi \qquad (4.16c)$$

(b) n is even

$$I_{Nq} = -2j\cos\frac{n\pi}{2}\, e^{-j\beta_o h} \int_o^h J'_n(k_{cq}r)\sin\beta_o r\, dr \qquad (4.17a)$$

$$e_{rq} = J'_n(k_{cq}r)\cos n\phi \qquad (4.17b)$$

$$e_{\phi q} = -\frac{n}{k_{cq}}\ \frac{J_n(k_{cq}r)}{r}\sin n\phi \qquad (4.17c)$$

While I_{Dq} is given in eq. (4.11).

Equations (4.12) to (4.17) give the proper expressions for I_{Nq} and the fields in an open-cavity radiator with a transmission

line exciter. The integrations for I_{Nq} can be carried out numerically by a computer.

4.2.3 Radiation Resistance

In Chapter 2, the radiation resistance of the primary radiator has been obtained by calculating the total radiated power and then dividing it by a half of the square of the input current of the primary radiator. For the case of a transmission line exciter, the radiation resistance is different from the input resistance because of the presence of the terminal impedance Z^t. The formula we derived in Chapter 2 gives only the radiation resistance.

From the equivalent circuit of this transmission line in Fig. 4.1(b), the input impedance of the exciter may be expressed as

$$Z_{in} = \frac{P_\ell + 2j\omega(W_m - W_e)}{\frac{1}{2} I_o I_o^*} \tag{4.18}$$

where P_ℓ is the real power radiated by the radiator plus the loss in the terminal resistor, and $(W_m - W_e)$ is the stored energy in the transmission line, the cavity and the transmission line terminator.

If we define the radiation and terminal resistance as R^r and R^t, respectively, then the real power, P_ℓ, is equal to

$$P_\ell = \frac{1}{2} I_o I_o^* R^r + \frac{1}{2} I(h) I^*(h) R^t \tag{4.19}$$

The first part of P_ℓ is the radiated power and is the same as that defined in Chapter 2, therefore the theoretical radiation resistance

can be calculated from eq. (2.29). The second part of P_ℓ can be calculated based on the wire current expressed in eq. (4.1) and a measured value of the terminal resistance R^t. In this case, it is found that the loss due to the radiation is small compared with the loss at the terminal resistor. In other words, R^r is small compared with R^t.

4.3 Comparison between Theoretical and Experimental Results

The experimental setup for measuring the radiation field and the input impedance of an open-cavity radiator with a transmission line exciter is almost identical to the setup used for the case of a radiator with a dipole exciter. A GR precision slotted line is used to substitute the balun and the shield pair line for measuring the input impedance.

In the course of measuring the input impedance, we can only measure the total input impedance which includes the impedances due to radiation and due to termination of the transmission line. To measure the radiation resistance we conduct one more experiment as follows: The open end of the open-cavity radiator is covered by a perfect conducting plate and the length of cavity is properly adjusted to avoid the resonance. The input resistance under this condition should be due to the loss at the terminal resistor of the transmission line only. If the total length of the transmission line is half wave length, the difference between two measured resistances mentioned above is the radiation resistance of the primary radiator.

Table 4.1 shows the experimental and theoretical radiation resistances as functions of the cavity length

Table 4.1 Experimental and Theoretical Radiation Resistance of an Open-Cavity Radiator with a Transmission Line Exciter $\ell_1 = 0.045\,\lambda_o$, $2h = 0.5\,\lambda_o$.

$L=\ell_1+\ell_2$ (in λ_o)	Theoretical Radiation Resistance	Experimental Radiation Resistance
0.6	5.13	7.6
0.8	6.17	9.1
1.0	7.58	9.6
1.2	5.14	6.6
1.4	4.92	4.7
1.6	5.93	8.1
1.8	6.72	9.1
2.0	6.50	8.5
2.2	5.50	7.6

The theoretical results of the radiation patterns of an open-cavity radiator with a transmission line exciter are obtained from the formulas in Chapter 2, while the experimental results are measured by a setup discussed in Chapter 3. Since the spacing between the conductor and the shorted end of the cavity is kept small, only the case of $\ell_1 = 0.045\,\lambda_o$ is considered. In Figs. (4.2) to (4.4), the theoretical (dotted line) and experimental (solid line) results are presented and compared. In these figures, the transmission line has a length of $0.5\,\lambda_o$ and the dimensions of the cavity are the same as the previous case in Chapter 3. A satisfactory agreement was obtained between theory and experiment.

4.4 Conclusion

In this study, the radiation fields and the radiation resistance of an open-cavity radiator with a transmission line exciter have been obtained theoretically and experimentally. A satisfactory agreement between theory and experiment confirm the accuracy of the present theoretical analysis.

For the radiation patterns a better agreement between theory and experiment is obtained for the case of a longer cavity length. The small value of the radiation resistance of this radiator suggests a low radiation efficiency. The strong point of this radiator is its broadband nature. Because of the resitance termination of the transmission line exciter, the input impedance of this radiator is quite frequency independent.

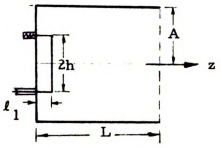

$A = 1.0\ \lambda_o$

$2h = 0.5\ \lambda_o$

$\ell_1 = 0.045\ \lambda_o$

$L = \ell_1 + \ell_2 = 0.8\ \lambda_o$

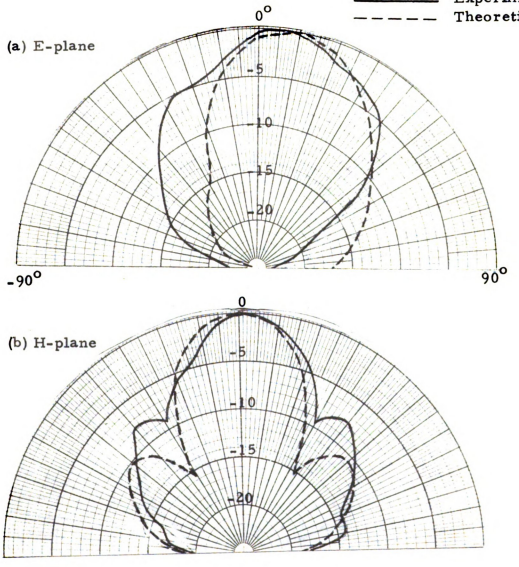

Fig. 4.2 Radiation patterns of the open-cavity radiator with a transmission line exciter at $L = 0.8\ \lambda_o$.

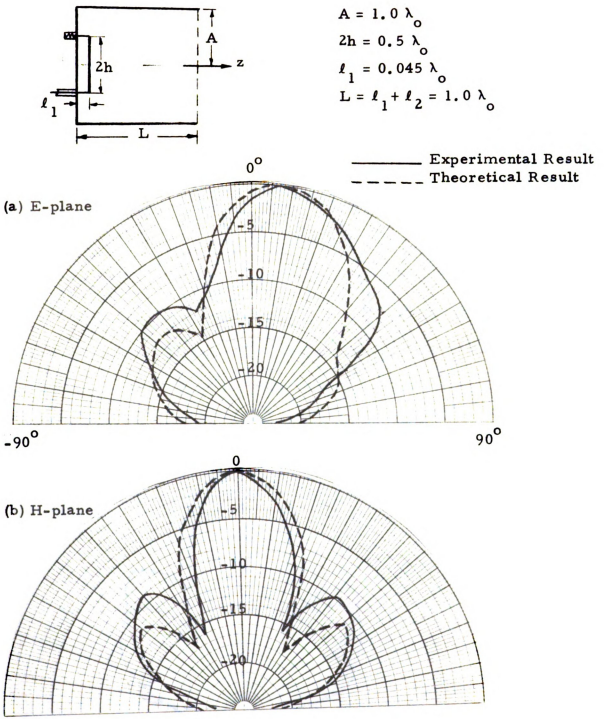

Fig. 4.3 Radiation patterns of the open-cavity radiator with a transmission line exciter at $L = 1.0\ \lambda_o$.

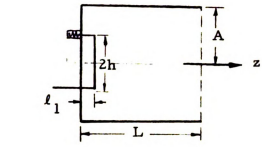

$A = 1.0\ \lambda_o$
$2h = 0.5\ \lambda_o$
$\ell_1 = 0.045\ \lambda_o$
$L = \ell_1 + \ell_2 = 1.2\ \lambda_o$

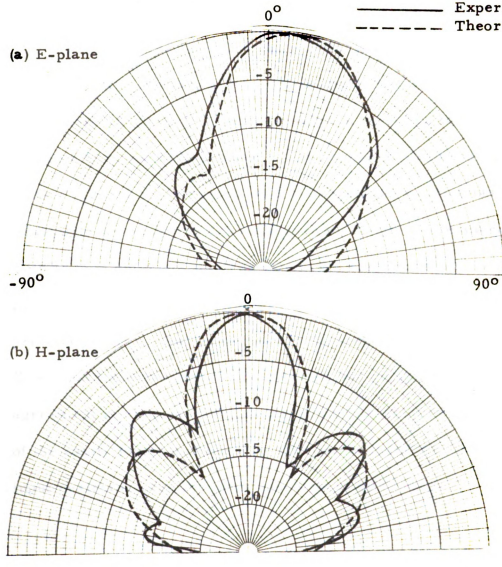

Fig. 4.4 Radiation patterns of the open-cavity radiator with a transmission line exciter at $L = 1.2\ \lambda_o$.

CHAPTER 5

OPEN-CAVITY RADIATORS WITH CIRCULAR LOOP EXCITERS

5.1 Introduction

This chapter is devoted to investigate the radiation fields and the input resistance of an open-cavity radiator excited by a circular loop. A circular loop is assumed to be either in a transverse plane or in a longitudinal plane. The waveguide excitation theory and Stokes' theorem are used to find the expansion coefficients of the waveguide modes which are excited in the cavity. The aperture field is then determined. The expansion coefficients of the propagating modes are also used to determine the input resistance of the primary exciter. Experimental and theoretical results for radiation fields and input resistance are obtained and compared. A satisfactory agreement is obtained between theory and experiment. The effects of the cavity length and the loop size on the radiation fields and the input resistance are the main concerns of this analysis.

5.2 Expansion Coefficients and Input Resistance of an Open-Cavity Radiator with a Circular Loop Exciter Placed in a Transverse Plane

5.2.1 Geometry

Figure 5.1 shows the geometry of an open-cavity radiator with a circular loop exciter placed in the transverse plane. The loop is made of a thin conducting wire with a radius of d. The loop is located in a transverse plane at z = 0 and with its center on the z-axis. A cylindrical coordinate (r, ϕ, z) is used in the analysis. The current distribution for this circular loop can be mathematically expressed as

$$\vec{J}_a = \hat{\phi}\,\frac{I_o \cos\beta_o d(\pi - |\phi|)}{\cos\beta_o d\,\pi}\,\delta(r-d)\delta(z) \qquad -\pi \le \phi \le \pi \qquad (5.1)$$

where I_o is the input current at (d, 0, 0) and β_o is the wave number in the free-space.

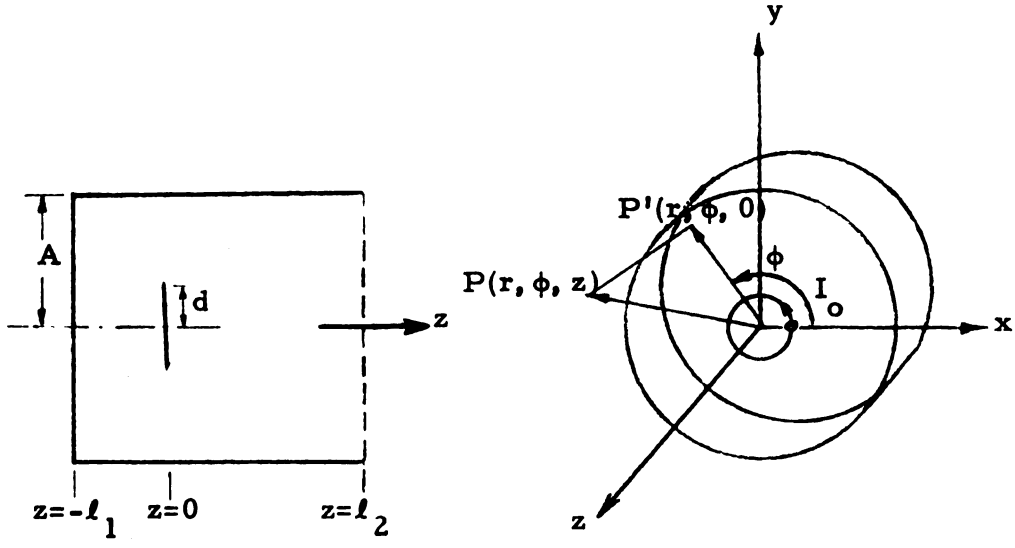

Fig. 5.1 Geometry of an open-cavity radiator with a circular loop exciter placed in a transverse plane.

The circular cavity is the same as that defined in Chapter 2. This cavity is shorted at $z = -\ell_1$ and has an open end at $z = \ell_2$.

5.2.2 Expansion Coefficients

The expressions for the expansion coefficients for the q th waveguide mode in the open-cavity radiator are

$$B_q = \frac{\Gamma_{2q} M_q + N_q}{\Gamma_{1q}\Gamma_{2q} - 1}$$

$$C_q = \frac{\Gamma_{1q} N_q + M_q}{\Gamma_{1q}\Gamma_{2q} - 1}$$

where

$$M_q = \frac{Z_q \int_v \vec{E}_q^- \cdot \vec{J}_a \, dv}{2\int_{c.s.} (\vec{e}_q \cdot \vec{e}_q) ds} \quad \text{and} \quad N_q = \frac{Z_q \int_v \vec{E}_q^+ \cdot \vec{J}_a \, dv}{2\int_{c.s.} (\vec{e}_q \cdot \vec{e}_q) ds}$$

The numerators of M_q and N_q for the case of a circular loop placed in a transverse plane can be found as

$$\int_v \vec{E}_q^- \cdot \vec{J}_a \, dv = \frac{I_o}{\cos\beta_o d\pi} \int_{-\ell_1}^{\ell_2} \int_{c.s.} (\vec{e}_q - \vec{e}_{zq}) e^{j\beta_g z} \cdot \hat{\phi} \cos\beta_o d(\pi - |\phi|) \cdot \delta(r-d)\delta(z) ds \, dz$$

$$= \frac{I_o}{\cos\beta_o d\pi} \int_0^A \int_{-\pi}^{\pi} e_{q\phi} \cos\beta_o d(\pi - |\phi|) \delta(r-d) r \, d\phi \, dr$$

$$= \frac{I_o}{\cos\beta_o d\pi} \int_{-\pi}^{\pi} e_{q\phi}(r=d) \cos\beta_o d(\pi - |\phi|) d \, d\phi \qquad (5.2)$$

and

$$\int_v \vec{E}_q^+ \cdot \vec{J}_a \, dv = \int_v \vec{E}_q^- \cdot \vec{J}_a \, dv = \frac{I_o}{\cos\beta_o d\pi} \int_{-\pi}^{\pi} e_{q\phi}(r=d) \cos\beta_o d(\pi - |\phi|) d \, d\phi \qquad (5.3)$$

This leads to $M_q = N_q$ and then C_q can be obtained as

$$C_q = N_q \frac{\Gamma_{1q}+1}{\Gamma_{1q}\Gamma_{2q}-1} = \frac{I_o Z_q d}{2\cos\beta_o d\pi} \frac{\Gamma_{1q}+1}{\Gamma_{1q}\Gamma_{2q}-1} \frac{I_{Nq}}{I_{Dq}} \tag{5.4}$$

where

$$I_{Nq} = \int_{-\pi}^{\pi} e_{q\phi}(r=d)\cos\beta_o d(\pi-|\phi|)d\phi \tag{5.5}$$

and

$$I_{Dq} = \int_{c.s.} (\vec{e}_q \cdot \vec{e}_q)ds = \int_0^A \int_{-\pi}^{\pi} [(e_{rq})^2 + (e_{\phi q})^2]\, r\, d\phi\, dr \tag{5.6}$$

The value of I_{Dq} is the same as that obtained in Chapter 3. I_{Nq} should be evaluated separately for the TE and TM modes.

(i) TE Modes:

The transverse electric fields for the q th TE mode are

$$e_{rq} = \frac{n}{k_{cq} r} J_n(k_{cq} r)\sin n\phi \tag{5.7a}$$

$$e_{\phi q} = J_n'(k_{cq} r)\cos n\phi \tag{5.7b}$$

Substituting eqs. (5.7) into eqs. (5.5) and (5.6), I_{Nq} and I_{Dq} can be obtained as

$$I_{Nq} = \int_{-\pi}^{\pi} J_n'(k_{cq} d)\cos n\phi \cos\beta_o d(\pi-|\phi|)d\phi$$

$$= J_n'(k_{cq} d)\Big[\cos\beta_o d\pi \int_{-\pi}^{\pi} \cos\beta_o d\phi \cos n\phi d\phi + \sin\beta_o d\pi \int_{-\pi}^{\pi} \sin\beta_o d|\phi| \cdot \cos n\phi\, d\phi\Big]$$

$$= \frac{2\beta_o d}{(\beta_o d)^2 - n^2} \sin\beta_o d\pi\, J_n'(k_{cq} d) \tag{5.8}$$

and

$$I_{Dq} = \pi \int_0^A \left[\frac{n^2}{k_{cq}^2 r} J_n^2(k_{cq} r) + r J_n'^2(k_{cq} r) \right] dr \qquad (5.9)$$

(ii) TM Modes:

The transverse electric fields for the qth TM mode are:

$$e_{rq} = J_n'(k_{cq} r) \sin n\phi \qquad (5.10a)$$

$$e_{\phi q} = \frac{n}{k_{cq} r} J_n(k_{cq} r) \cos n\phi \qquad (5.10b)$$

Therefore, I_{Nq} and I_{Dq} for the TM mode can be evaluated to be

$$I_{Nq} = \int_{-\pi}^{\pi} \frac{n}{k_{cq} d} J_n(k_{cq} d) \cos n\phi \cos\beta_o d(\pi - |\phi|) d\phi$$

$$= \frac{2n\beta_o}{k_{cq}[(\beta_o d)^2 - n^2]} \sin\beta_o d\pi \, J_n(k_{cq} d) \qquad (5.11)$$

and

$$I_{Dq} = \pi \int_0^A \left[\frac{n^2}{k_{cq}^2 r} J_n^2(k_{cq} r) + r J_n'^2(k_{cq} r) \right] dr \qquad (5.12)$$

Up to this point, I_{Nq} and I_{Dq} for the TE and TM modes are evaluated. The calculations of I_{Nq} and I_{Dq} are carried out numerically by a CDC 6500 computer.

5.2.3 Input Resistance

After the expansion coefficients are completely determined, the input resistance of the loop can be obtained by using eq. (2.29) developed in Chapter 2.

5.3 Expansion Coefficients and Input Resistance of an Open-Cavity Radiator with a Circular Loop Exciter Placed in a Longitudinal Plane

5.3.1 Geometry and Expansion Coefficients

Figure 5.2(a) shows the geometry of an open-cavity radiator with a circular loop located in the y-z plane or a longitudinal plane. The circular loop has a radius of d and its center is located at the origin of the cylindrical coordimates (r, ϕ, z). The cavity is the same as the previous case and it is shorted at $z = -\ell_1$ and open at $z = \ell_2$.

A new cylindrical coordinate system (r', θ, x) is used to describe the circular loop exciter as shown in Fig. 5.2(b). For simplicity, the radius of the circular loop is assumed to be small compared with the wavelength. The current $\vec{J}_a$ for such a small loop can be assumed to be

$$\vec{J}_a = I_o \, \delta(r'-d)\delta(x)\,\hat{\theta} \tag{5.13}$$

where I_o is the input current at $(d, -\frac{\pi}{2}, 0)$. The case of a more general current distribution on a larger loop will not be considered here to avoid mathematical complexity.

In order to find the expression for C_q, M_q and N_q are evaluated first. Substituting eq. (5.13) into the expressions for M_q and N_q, we have

$$\int_v \vec{E}_q^{+} \cdot \vec{J}_a \, dv = I_o \int_{-\ell_1}^{\ell_2} \int_0^{2\pi} \int_0^{A} \vec{E}_q^{+} \cdot \hat{\theta}\, \delta(r'-d)\delta(x) r' dr' d\theta\, dx$$

$$= I_o \oint_c \vec{E}_q^{+} \cdot \hat{\theta}\, d\, d\theta = I_o \oint_c \vec{E}_q^{+} \cdot d\vec{\ell} \tag{5.14}$$

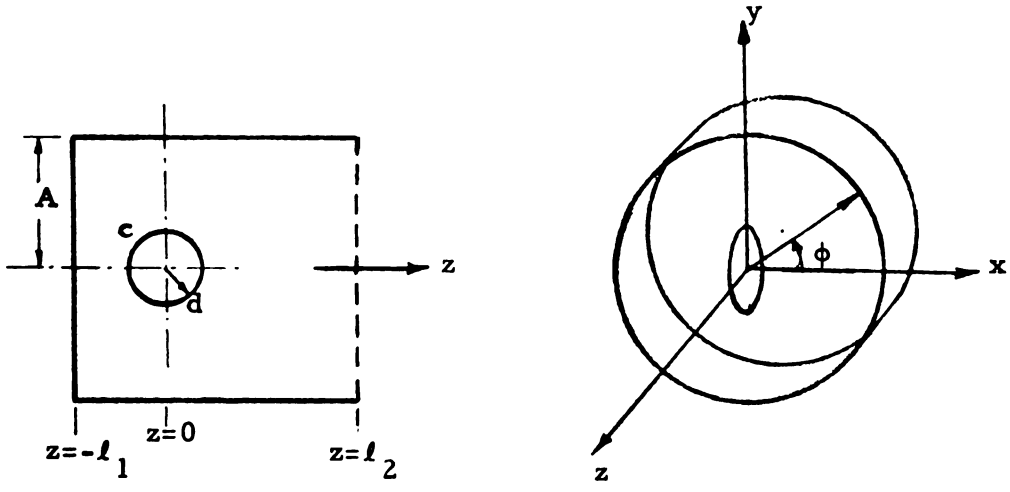

(a) Geometry of the radiator

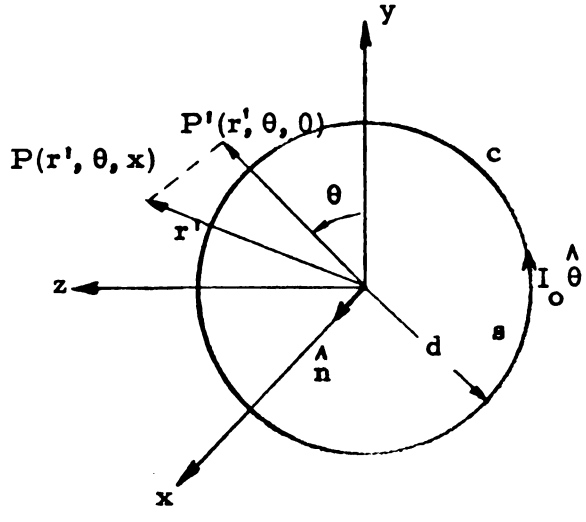

(b) Geometry of the circular loop exciter

Fig. 5.2 Geometries of an open-cavity radiator with a circular loop exciter placed in a longitudinal plane.

where

$$\vec{d\ell} = d \cdot d\theta \, \hat{\theta}$$

Using Stokes' Theorem and a Maxwell equation, eq. (5.14) becomes

$$\int_v \vec{E}_q^+ \cdot \vec{J}_a dv = I_o \oint_c \vec{E}_q^+ \cdot \vec{d\ell} = I_o \int_s (\nabla \times \vec{E}_q) \cdot ds$$

$$= -j\omega\mu I_o \int_s \vec{H}_q^+ \cdot \hat{n} \, ds \qquad (5.15)$$

where s is the total area enclosed by the loop c and $\hat{n} = \hat{x}$ or the unit vector normal to s.

Similarly, we get

$$\int_v \vec{E}_q^- \cdot \vec{J}_a dv = -j\omega\mu I_o \int_s \vec{H}_q^- \cdot \hat{n} ds \qquad (5.16)$$

$\vec{H}_q^{\pm}$ has been defined in Chapter 2 as

$$\vec{H}_q^{\pm} = (\pm \vec{h}_q + \vec{h}_{zq}) e^{\mp j\beta_q z} \qquad (2.2b)$$

Therefore C_q can be rewritten as

$$C_q = \frac{\Gamma_{1q} N_q + M_q}{\Gamma_{1q}\Gamma_{2q} - 1} = \frac{-j\omega\mu I_o Z_q}{(\Gamma_{1q}\Gamma_{2q} - 1) \cdot 2 \int_{c.s.} \vec{e}_q \cdot \vec{e}_q ds} \left[\Gamma_{1q} \int_s \vec{h}_q e^{-j\beta_q z} \cdot \hat{x} \, ds \right.$$

$$\left. - \int_s \vec{h}_q \, e^{j\beta_q z} \cdot \hat{x} \, ds \right] \qquad (5.17)$$

Since $\vec{h}_q$ is a function of r and ϕ only, the integration with respect to z can be simplified and C_q becomes

$$C_q = \frac{j\omega\mu\, I_o Z_q (1-\Gamma_{1q})}{2\int_{c.s.} (\vec{e}_q \cdot \vec{e}_q) ds (\Gamma_{1q}\Gamma_{2q} - 1)} \int_s \vec{h}_q \cos\beta_q z \cdot \hat{x}\, ds$$

$$= \frac{j\omega\mu_o I_o Z_q (1-\Gamma_{1q})}{2(\Gamma_{1q}\Gamma_{2q} - 1)} \frac{I_{Nq}}{I_{Dq}} \tag{5.18}$$

where I_{Nq} and I_{Dq} are defined as

$$I_{Nq} = \int_s \vec{h}_q \cos\beta_q z \cdot \hat{x}\, ds \tag{5.19a}$$

and

$$I_{Dq} = \int_{c.s.} (\vec{e}_q \cdot \vec{e}_q) ds \tag{5.19b}$$

The value of I_{Dq} is the same as that in the previous chapter, but the calculation for I_{Nq} is quite complicated. In the cylindrical coordinates (r, ϕ, z), $x = r\cos\phi = 0$ implies that $\phi = (2n-1)\pi/2$ where n is the integer. Also $\hat{x}$ and $\vec{h}_q$ can be expressed as

$$\hat{x} = \hat{r}\cos\phi - \hat{\phi}\sin\phi \tag{5.20a}$$

$$\vec{h}_q = \hat{r} h_{rq} + \hat{\phi} h_{\phi q} \tag{5.20b}$$

Therefore, the scalar product of $\vec{h}_q \cdot \hat{x}$ on the S surface is equal to

$$\vec{h}_q \cdot \hat{x}\Big|_{\text{on S}} = \vec{h}_q(x=0) \cdot \hat{x} = (h_{rq}\cos\phi - h_{\phi q}\sin\phi)\Big|_{\phi=\frac{(2n-1)}{2}\pi}$$

$$= -\, h_{\phi q}\sin\phi\Big|_{\phi=\frac{(2n-1)}{2}\pi} \tag{5.21}$$

Since $r = x\cos\phi + y\sin\phi$, we have

$$\begin{cases} \phi = \dfrac{\pi}{2} & r = y \\ \phi = \dfrac{3\pi}{2} & r = -y \end{cases} \tag{5.22}$$

Refer to Fig. 5.2(b), r' along the path C is expressed by

$$r'^2 = y^2 + z^2 = d^2$$

or

$$z = \pm \sqrt{d^2 - y^2} \tag{5.23}$$

Substituting the above relations in the expression for I_{Nq}, it leads to

$$I_{Nq} = \int_s \vec{h}_q \cdot \cos\beta_q z \cdot \hat{x}\, ds$$

$$= -\int_o^d \int_{-\sqrt{d^2-y^2}}^{\sqrt{d^2-y^2}} h_{\phi q}(\phi=\tfrac{\pi}{2}, r=y)\cos\beta_q z\, dz\, dy + \int_{-d}^{o} \int_{-\sqrt{d^2-y^2}}^{\sqrt{d^2-y^2}} h_{\phi q}(\phi=\tfrac{\pi}{2}, r=-y) \cdot \cos\beta_q z\, dz\, dy$$

$$= \frac{2}{\beta_q} \int_o^d [\, h_{\phi q}(\phi=\tfrac{3\pi}{2}) - h_{\phi q}(\phi=\tfrac{\pi}{2})] \sin\beta_q \sqrt{d^2-y^2}\, dy \tag{5.24}$$

The final expressions for the expansion coefficients C_q for the TE and TM modes are obtained as follows:

(i) TE Modes:

The fields for the q th TE mode are

$$h_{rq} = -\frac{1}{Z_q} J'_n(k_{cq} r)\cos n\phi$$

$$h_{\phi q} = \frac{n}{Z_q k_{cq}} \frac{J_n(k_{cq} r)}{r} \sin n\phi$$

I_{Nq} for the TE mode can be obtained as

$$I_{Nq} = \frac{2}{\beta_q} \cdot \frac{n}{Z_q k_{cq}} (\sin\tfrac{3n\pi}{2} - \sin\tfrac{n\pi}{2}) \int_o^d \frac{J_n(k_{cq} y)}{y} \sin\beta_q \sqrt{d^2-y^2}\, dy$$

$$= -\frac{4n \sin\frac{n\pi}{2}}{\beta_q Z_q k_{cq}} \int_o^d \frac{J_n(k_{cq} y)}{y} \sin\beta_q \sqrt{d^2-y^2}\, dy \tag{5.25}$$

With $Z_q = \omega\mu/\beta_q$, C_q for the q th TE mode becomes

$$C_q = j2nI_o \frac{Z_q \sin(n\pi/2)}{k_{cq} I_{Dq}} \cdot \frac{\Gamma_{1q} - 1}{\Gamma_{1q}\Gamma_{2q} - 1} \int_o^d \frac{J_n(k_{cq} y)}{y} \sin\beta_q \sqrt{d^2 - y^2}\, dy \tag{5.26}$$

(ii) TM Modes:

The fields for the q th TM mode are

$$h_{rq} = -\frac{n}{Z_q} \frac{J_n(k_{cq} r)}{k_{cq} r} \cos n\phi$$

$$h_{\phi q} = \frac{1}{Z_q} J'_n(k_{cq} r) \sin n\phi$$

Following the same process as in the TE mode case, I_{Nq} and C_q for the q th TM mode can be obtained as

$$I_{Nq} = -\frac{4 \sin\frac{n\pi}{2}}{\beta_q Z_q} \int_o^d J'_n(k_{cq} y) \sin\beta_q \sqrt{d^2 - y^2}\, dy \tag{5.27}$$

and

$$C_q = j2I_o \frac{Z_o^2}{Z_q^2} \frac{\sin(n\pi/2)}{I_{Dq}} \frac{\Gamma_{1q} - 1}{\Gamma_{1q}\Gamma_{2q} - 1} \int_o^d J'_n(k_{cq} y) \sin\beta_q \sqrt{d^2 - y^2}\, dy \tag{5.28}$$

Up to this point, the expansion coefficients C_q for the TE and TM modes are completely determined.

5.3.2 Input Resistance

After the expansion coefficients are completely determined, the input resistance can be evaluated using eq. (2.29) developed in Chapter 2.

5.4 Comparison between Theory and Experiment

In this section, theoretical and experimental results of the radiation patterns and the input resistance for an open-cavity radiator with a circular loop exciter placed in a transverse plane or in a longitudinal plane are obtained and compared. The experimental input resistance for the case of a small loop placed in a longitudinal plane is not presented here because it is so small that it is very hard to conduct the measurement.

Figures 5.3 to 5.8 show the radiation patterns of open-cavity radiators with various cavity length and two different circular loops placed in transverse planes of the cavity. The theoretical results (dotted line) and experimental results (solid line) are plotted together for easy comparison. The E-plane ($\phi=90^{o}$) and H-plane ($\phi=0^{o}$) radiation patterns are presented in these figures. In all these figures, a satisfactory agreement between theory and experiment is obtained.

Figures 5.3 to 5.5 show the radiation patterns of the radiators with a circular loop of $0.09\ \lambda_o$ radius and placed at $0.25\ \lambda_o$ from the shorted end of the cavity, and with the cavity length of $0.8\ \lambda_o$ $1.0\ \lambda_o$ and $1.2\ \lambda_o$, respectively. Figures 5.6 to 5.8 show the radiation patterns of the three radiators treated in Figs. 5.3 to 5.5 but the size of the circular loop is increased to have a $0.19\ \lambda_o$ radius. Comparing Figs. 5.3 to 5.5 with Figs. 5.6 to 5.8, it is observed that the effect of the size of the loop exciter on the radiation patterns seems

rather significant. It is also observed that in the case of a larger loop exciter, the effect of the cavity length on the H-plane pattern is found to be quite outstanding.

Since the theoretical analysis on the radiation and circuit properties of an open-cavity radiator with a circular loop exciter placed in a longitudinal plane is based on the assumption that the loop is small and has a uniform current distribution, only the case of a small loop with a radius of 0.06 λ_o is investigated. Figures 5.9 to 5.11 give theoretical and experimental radiation patterns of the radiators with a small circular loop as mentioned above. The center of the loop is placed at 0.25 λ_o away from the shorted end of the cavity and the cavity lengths are set to be 0.8 λ_o, 1.0 λ_o, and 1.2 λ_o, respectively. It is observed that the radiation patterns in these figures are broader than those produced with a loop placed in a transverse plane.

The experimental results on the input resistance of an open-cavity radiator with a loop placed in a transverse plane are compared with the theoretical results. Table 5.1 shows the comparison between theoretical input resistance and experimental input impedance of a radiator with dimensions specified in Fig. 5.3 and with the cavity length varied from 0.6 λ_o to 1.2 λ_o. Table 5.2 gives the same comparison for a radiator described in Fig. 5.6. In these two tables, a qualitative agreement is obtained between theory and experiment. The agreement is better for the case of a larger loop exciter.

The theoretical input resistance of an open-cavity radiator with a small circular loop exciter placed in a longitudinal plane is very small. It ranges from one to three ohms when the radius of the loop is $0.06\ \lambda_o$ and the cavity length is varied from $0.6\ \lambda_o$ to $1.2\ \lambda_o$. It is very hard, if not impossible, to measure this small input resistance using a conventional driving line. For this reason, no experimental input resistance is available for comparison with theoretical results.

Table 5.1 Experimental Input Impedance and Theoretical Input Resistance of an Open-Cavity Radiator with a Circular Loop Exciter Placed in a Transverse Plane, $d = 0.09\ \lambda_o$, $\ell_1 = 0.25\ \lambda_o$.

Cavity Length $L = \ell_1 + \ell_2$	Experimental Input Impedance	Theoretical Input Resistance
$0.6\ \lambda_o$	330.4 + j481.7	484.1
$0.8\ \lambda_o$	344.3 + j411.6	557.9
$1.0\ \lambda_o$	406.7 + j381	671.3
$1.2\ \lambda_o$	315.8 + j356.2	481.6

Table 5.2 Experimental Input Impedance and Theoretical Input Resistance of an Open-Cavity Radiator with a Circular Loop Exciter Placed in a Transverse Plane, $d = 0.19\ \lambda_o$, $\ell_1 = 0.25\ \lambda_o$.

Cavity Length	Experimental Input Impedance	Theoretical Input Resistance
$0.6\ \lambda_o$	259.0 + j253.6	292.9
$0.8\ \lambda_o$	342.7 + j190.5	362.3
$1.0\ \lambda_o$	373.6 + j95.2	446.3
$1.2\ \lambda_o$	254.0 + j152.9	309.9

5.5 Conclusion

A theoretical analysis on the radiation and circuit properties of an open-cavity radiator with a circular loop exciter placed in a longitudinal plane or in a transverse plane has been presented in this chapter. Most of the theoretical results have been confirmed by the experimental results.

Concerning the radiation patterns, some facts of significance are pointed out as follows: (a) The E-plane radiation pattern of the radiator is quite independent of the cavity length when the exciter is placed in a transverse plane. (b) The cavity length has a rather significant effect on the H-plane pattern. (c) The size of the circular loop exciter when placed in a transverse plane tends to have a rather significant effect on the radiation characteristics of the radiator. It appears that a good radiation pattern can be realized by a proper choice of a loop exciter. (d) For the radiation with a circular loop exciter placed in a longitudinal plane, the radiation resistance is usually small and the radiation patterns are less directive. This radiator may have a less value in practical applications.

Among these figures on radiation patterns, rather large disagreements between theory and experiment are recorded in some cases. The sources of these disagreements are believed to be due to the same reasons mentioned in Sec. 3.6.

Concerning the input resistance of the radiator with a loop exciter placed in a transverse plane, theoretical input resistance

is in a qualitative agreement with the experimental input impedance. The agreement is better for the case of a larger loop exciter. Generally speaking, the input impedance is not strongly dependent on the cavity dimensions.

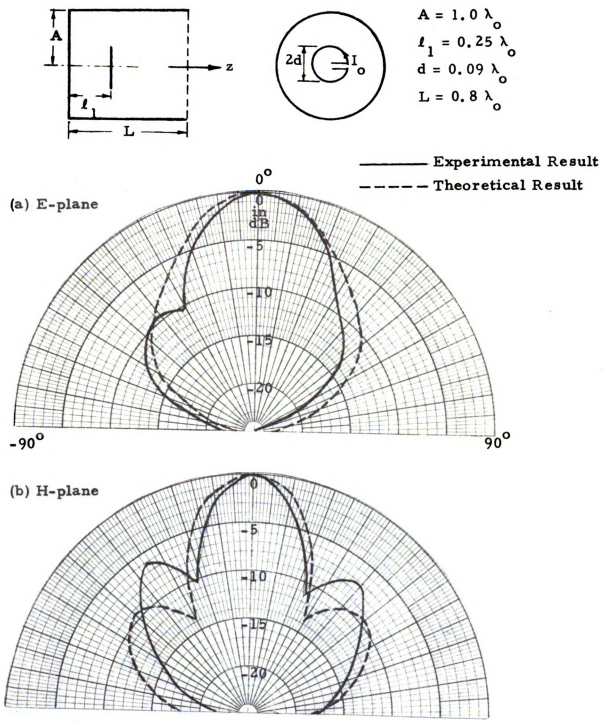

Fig. 5.3 Radiation patterns of an open-cavity radiator with a circular loop exciter placed in a transverse plane ($d = 0.09\,\lambda_o$, $L = 0.8\,\lambda_o$).

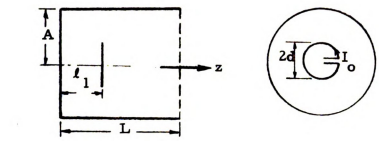

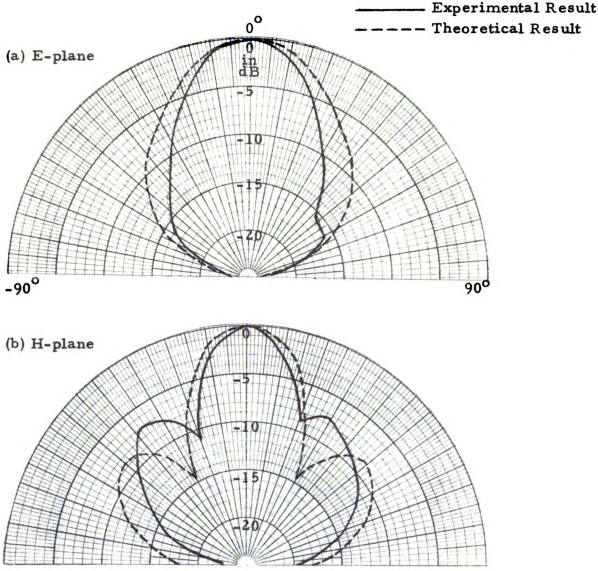

Fig. 5.4 Radiation patterns of an open-cavity radiator with a circular loop exciter placed in a transverse plane ($d = 0.09\,\lambda_o$, $L = 1.0\,\lambda_o$).

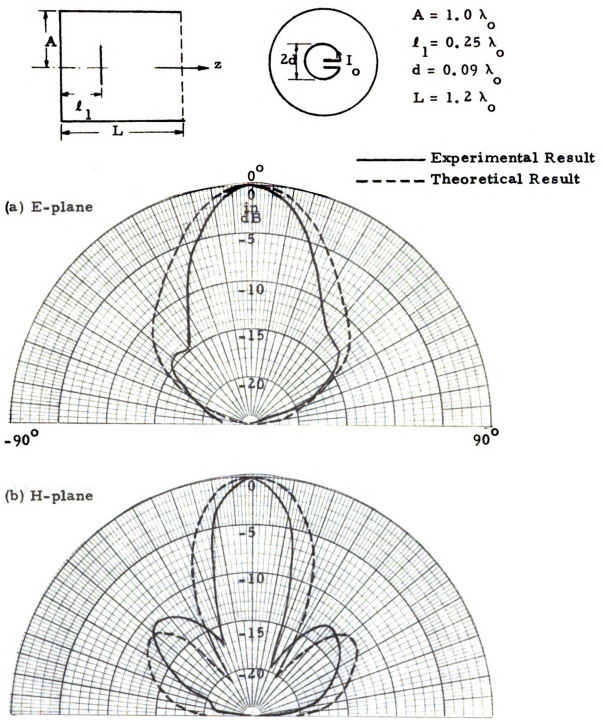

Fig. 5.5 Radiation patterns of an open-cavity radiator with a circular loop exciter placed in a transverse plane ($d = 0.09\,\lambda_o$, $L = 1.2\,\lambda_o$).

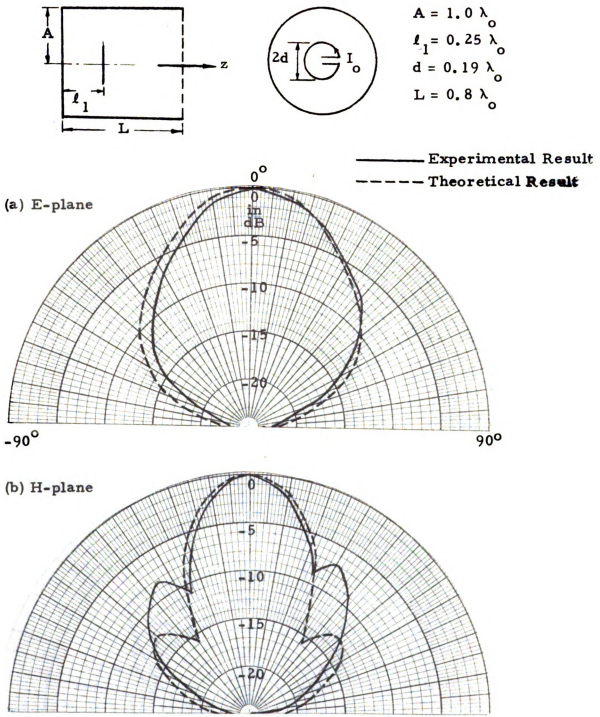

Fig. 5.6 Radiation patterns of an open-cavity radiator with a circular loop exciter placed in a transverse plane ($d = 0.19\,\lambda_o$, $L = 0.8\,\lambda_o$).

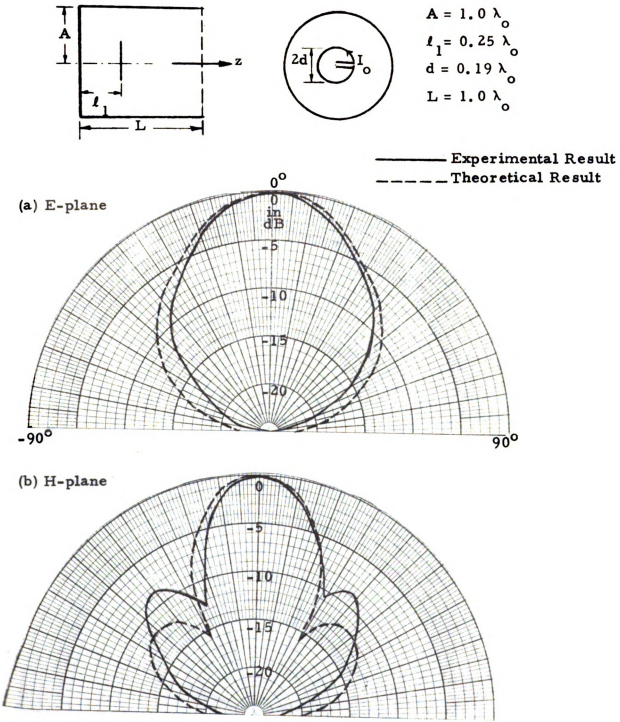

Fig. 5.7 Radiation patterns of an open-cavity radiator with a circuit loop exciter placed in a transverse plane ($d = 1.9\ \lambda_o$, $L = 1.0\ \lambda_o$).

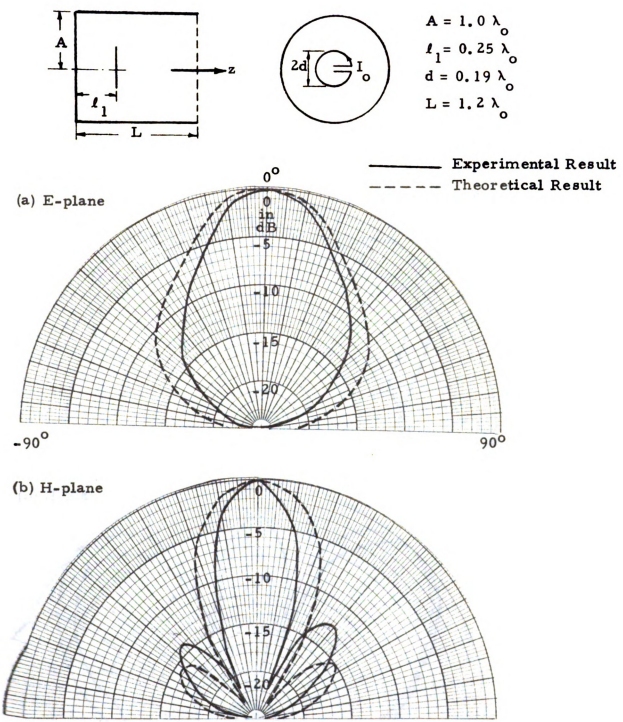

Fig. 5.8 Radiation patterns of an open-cavity radiator with a circular loop exciter placed in a transverse plane ($d = 0.19\,\lambda_o$, $L = 1.2\,\lambda_o$).

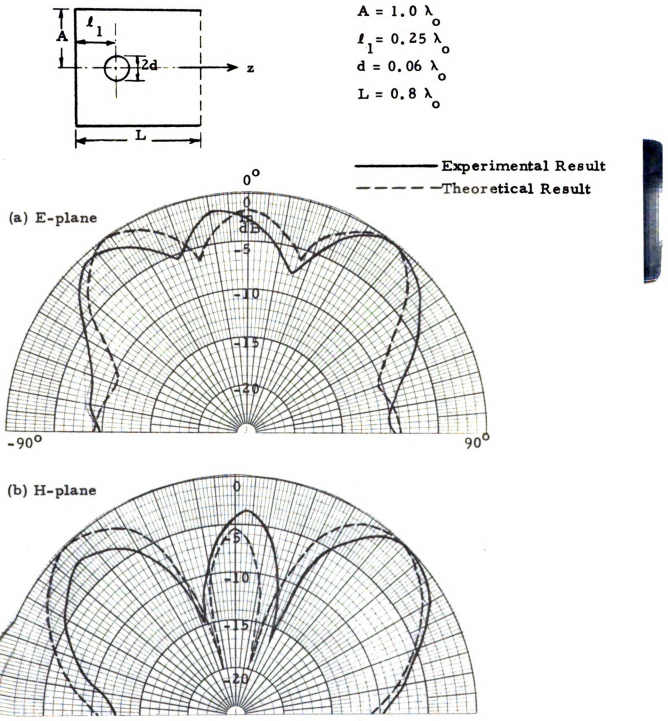

Fig. 5.9 Radiation patterns of an open-cavity radiator with a circular loop exciter placed in a longitudinal plane ($d = 0.06\ \lambda_o$, $L = 0.8\ \lambda_o$).

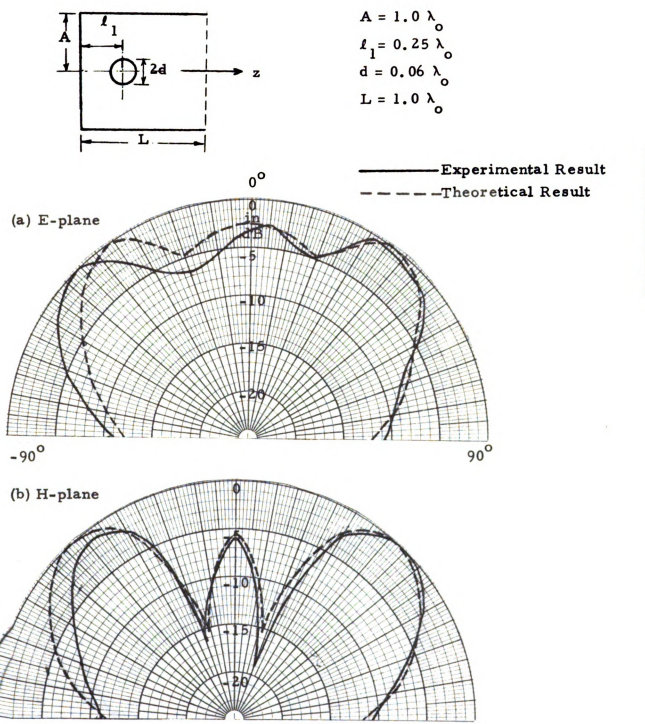

Fig. 5.10 Radiation patterns of an open-cavity radiator with a circular loop exciter placed in a longitudinal plane ($d = 0.06\ \lambda_o$, $L = 1.0\ \lambda_o$).

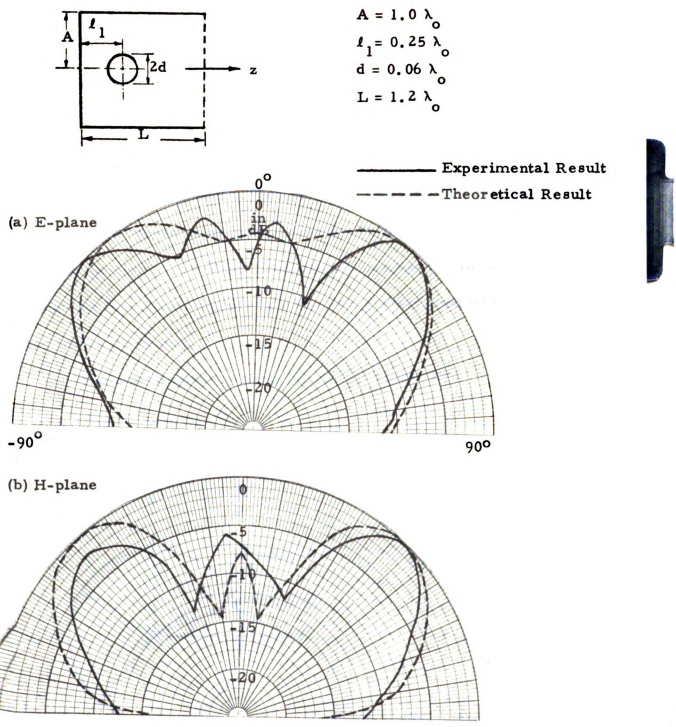

Fig. 5.11 Radiation patterns of an open-cavity radiator with a circular loop exciter placed in a longitudinal plane ($d = 0.06\ \lambda_o$, $L = 1.2\ \lambda_o$).

APPENDIX

NORMAL MODES IN CIRCULAR WAVEGUIDING STRUCTURE

Part I - Normal TE Modes

Figure A.1 shows the geometry of a cylindrical waveguide with a circular cross section of radius a. In view of the cylindrical geometry involved, cylindrical coordinates are used in the analysis. We assume that the waveguide is made of a perfect conductor and filled with a dielectric.

The general equations for TE, or H, modes are

$$\nabla_t^2 h_z + k_c^2 h_z = 0 \qquad \text{(A.1)}$$

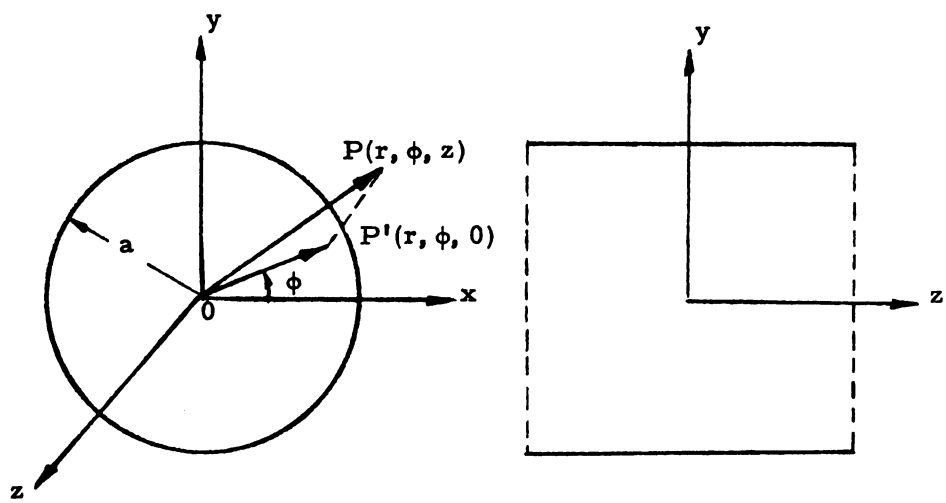

Fig. A.1 The circular cylindrical waveguide

where

$$k_c^2 = k^2 + \gamma^2 \tag{A.2}$$

and h_z in the longitudinal component of the H field in the waveguide. The transverse components are

$$\vec{h}_t = \mp \frac{\gamma}{k_c^2} \nabla_t h_z \tag{A.3}$$

$$\vec{e}_t = \pm Z^h \hat{z} \times \vec{h}_t \tag{A.4}$$

The boundary condition in this problem is

$$\frac{\partial h_z}{\partial n} (r=a) = 0 \tag{A.5}$$

where $k = \omega\sqrt{\mu\epsilon}$ is the propagation constant in the medium and $k_c = 2\pi f_c \sqrt{\mu\epsilon}$ is the cutoff wave number with f_c being the cutoff frequency for a certain waveguide mode. $Z^h = \frac{j\omega\mu}{\gamma}$ is the field impedance for TE modes and γ is the propagation constant for the waveguide mode.

Using the separation of variables method, a solution for eq. (A.1) is

$$h_z(r, \phi) = C J_n(k_c r) \begin{cases} \cos n\phi \\ \sin n\phi \end{cases} \tag{A.6}$$

where n is a positive integer. Subject to eq. (A.5), we have

$$\frac{\partial h_z}{\partial n} (r=a) = C' J_n'(k_c r) \begin{cases} \cos n\phi \\ \sin n\phi \end{cases} = 0$$

or

$$J_n'(k_c r) = 0 \tag{A.7}$$

Table A.1 below shows the ℓth root of $J_n'(p'_{n,\ell}) = 0$. The eigenvalues $k_{c,n\ell}$ are given by

$$k_{c,n\ell} = \frac{p'_{n\ell}}{a} \tag{A.8}$$

Table A.1 Values of $p'_{n,\ell}$ for TE Modes

ℓ	$p'_{o\ell}$	$p'_{1\ell}$	$p'_{2\ell}$	$p'_{3\ell}$	$p'_{4\ell}$	$p'_{5\ell}$	$p'_{6\ell}$
1	3.832	1.841	3.054	4.201	5.317	6.416	7.501
2	7.016	5.331	6.706	8.015	9.282	10.520	11.735
3	10.173	8.531	9.969	11.346	12.682	13.987	15.265
4	13.324	11.706	13.170	14.580	16.202	17.375	18.640

If q has been used as a mixed index of n, ℓ covering all of the TE modes and normalize the fields by $j\frac{\omega\mu}{k_{cq}} C_q = 1$, eqs. (A.3) and (A.4) will lead to

$$e_{rq} = \frac{n}{k_{cq}r} J_n(k_{cq}r) \begin{cases} \sin n\phi \\ -\cos n\phi \end{cases} \tag{A.9a}$$

$$e_{\phi q} = J_n'(k_{cq}r) \begin{cases} \cos n\phi \\ \sin n\phi \end{cases} \tag{A.9b}$$

$$h_{zq} = -j\frac{k_{cq}}{\omega\mu} J_n(k_{cq}r) \begin{cases} \cos n\phi \\ \sin n\phi \end{cases} \tag{A.9c}$$

$$h_{rq} = -\frac{1}{Z_q^h} J_n'(k_{cq}r) \begin{cases} \cos n\phi \\ \sin n\phi \end{cases} \tag{A.9d}$$

$$h_{\phi q} = \frac{n}{Z_q^h k_{cq}r} J_n(k_{cq}r) \begin{cases} \sin n\phi \\ -\cos n\phi \end{cases} \tag{A.9e}$$

The propagation constant, β_q, for the q th TE mode is

$$\gamma_q = (k_{cq}^2 - k^2)^{\frac{1}{2}} = j(k^2 - k_{cq}^2)^{\frac{1}{2}} = j\beta_q$$

or $$\beta_q = \omega(\mu\epsilon)^{\frac{1}{2}} \left[1 - \left(\frac{\omega_{cq}}{\omega}\right)^2 \right]^{\frac{1}{2}} = \beta \left[1 - \left(\frac{\omega_{cq}}{\omega}\right)^2 \right]^{\frac{1}{2}} \qquad \text{(A.10)}$$

The cutoff frequency and cutoff wavelength are

$$\omega_{cq} = k_{cq}(\mu\epsilon)^{-\frac{1}{2}} = v\frac{p'_q}{a} \qquad \text{(A.11)}$$

$$\lambda_{cq} = \frac{v}{f_{cq}} = \frac{2\pi a}{p'_q} \qquad \text{(A.12)}$$

where v is the velocity of light in the medium. The field impedance for this particular mode is

$$Z_q^h = \frac{j\omega\mu}{\gamma_q} = \frac{\omega\mu}{\beta}\left[1 - \left(\frac{\omega_{cq}}{\omega}\right)^2 \right]^{-\frac{1}{2}} = \zeta\left[1 - \left(\frac{\omega_{cq}}{\omega}\right)^2 \right]^{-\frac{1}{2}} = \zeta\frac{\beta}{\beta_q} \qquad \text{(A.13)}$$

where ζ is the field impedance of the medium. If the dielectric in the waveguide is air, then $\zeta = \zeta_o = 120\pi$ ohms.

Figure A.2 illustrates the field distribution of some TE modes in the guide. From these field distributions it is possible to determine a proper location to place the primary exciter. In general, the primary exciter is placed in a location in such a way that the field of the exciter matches best with the field of the desired waveguide mode.

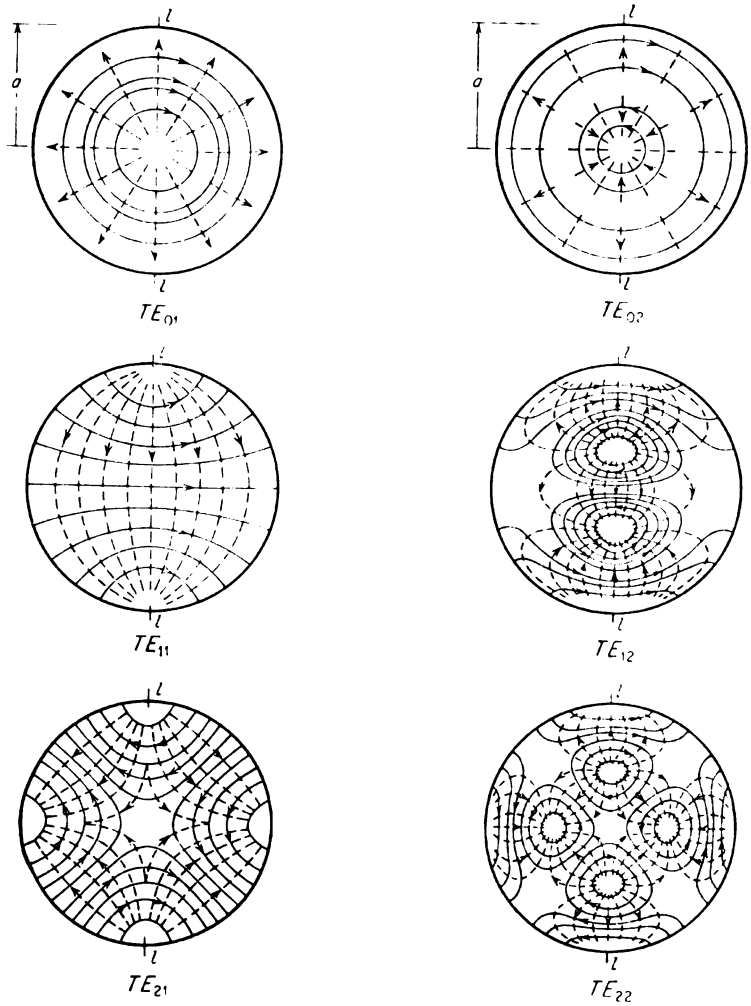

Fig. A.2. Field configurations in a circular waveguide for TE modes.

Part II - Normal TM Modes

The general equations for TM modes are

$$\nabla_t^2 e_z + k_c^2 e_z = 0 \tag{A.14}$$

where

$$k_c^2 = k^2 + \gamma^2 \tag{A.15}$$

The boundary condition is

$$e_z(r=a) = 0 \tag{A.16}$$

and the transverse fields are

$$\vec{e}_t = \mp \frac{\gamma}{k_c^2} \nabla_t e_z \tag{A.17}$$

$$\vec{h}_t = \pm \frac{1}{Z^e} \hat{z} \times \vec{e}_t \tag{A.18}$$

where

$$Z^e = \frac{\gamma}{j\omega\epsilon}$$

Using the same technique as for the TE modes we get

$$e_z(r, \phi) = D J_n(k_c r) \begin{cases} \cos n\phi \\ \sin n\phi \end{cases} \tag{A.19}$$

where D is a constant and n is a positive integer. The boundary condition, $e_z(r=a) = 0$, implies that $J_n(k_c a) = 0$.

Table A.2 below shows the ℓth root of $J_n(p_{n\ell}) = 0$. The eigenvalues $k_{c,\,n\ell}$ are given as

$$k_{c,\,n\ell} = \frac{p_{n\ell}}{a} \tag{A.20}$$

Table A.2 Value of $p_{n,\ell}$ for TM Modes

ℓ	$p_{o\ell}$	$p_{1\ell}$	$p_{2\ell}$	$p_{3\ell}$	$p_{4\ell}$	$p_{5\ell}$	$p_{6\ell}$
1	2.405	3.832	5.136	6.830	7.588	8.771	9.936
2	5.520	7.016	8.417	9.761	11.065	12.339	13.589
3	8.654	10.173	11.620	13.015	14.372	15.708	17.030
4	11.792	13.323	14.796	16.221	17.667	18.962	20.308

If q has been used as a mixed index of n, ℓ covering all of the qth TM modes and the fields are normalized by letting $\frac{\gamma_q D_q}{k_{cq}} = 1$, eqs. (A.17) and (A.18) become

$$e_{rq} = J_n'(k_{cq}r) \begin{cases} \cos n\phi \\ \sin n\phi \end{cases} \tag{A.21a}$$

$$e_{\phi q} = \frac{n}{k_{cq}r} J_n(k_{cq}r) \begin{cases} -\sin n\phi \\ \cos n\phi \end{cases} \tag{A.21b}$$

$$e_{zq} = -\frac{k_{cq}}{\gamma_q} J_n(k_{cq}r) \begin{cases} \cos n\phi \\ \sin n\phi \end{cases} \tag{A.21c}$$

$$h_{rq} = \frac{n}{k_{cq}r Z_q^e} J_n(k_{cq}r) \begin{cases} -\sin n\phi \\ \cos n\phi \end{cases} \tag{A.21d}$$

$$h_{\phi q} = -\frac{1}{Z_q^e} J_n'(k_{cq}r) \begin{cases} \cos n\phi \\ \sin n\phi \end{cases} \tag{A.21e}$$

The propagation constant, β_q, for the qth TM mode is,

$$\beta_q = (k^2 - k_{cq}^2)^{\frac{1}{2}} = \beta\left[1-\left(\frac{\omega_{cq}}{\omega}\right)^2\right]^{\frac{1}{2}} \tag{A.22}$$

The cutoff frequency ω_{cq} and cutoff wavelength λ_{cq} are

$$\omega_{cq} = k_{cq}(\mu\epsilon)^{-\frac{1}{2}} = vk_{cq} = v\frac{p_q}{a} \tag{A.23}$$

$$\lambda_{cq} = \frac{v}{f_{cq}} = \frac{2\pi f}{\omega_{cq}} = \frac{2\pi a}{p_q} \tag{A.24}$$

The field impedance of q th TM mode is defined as

$$Z_q^e = \frac{\gamma_q}{j\omega\epsilon} = \frac{\beta}{\omega\epsilon}\left[1 - \left(\frac{\omega_{cq}}{\omega}\right)^2\right]^{\frac{1}{2}} = \zeta\left[1 - \left(\frac{\omega_{cq}}{\omega}\right)^2\right]^{\frac{1}{2}} \tag{A.25a}$$

or $$Z_q^e = \frac{\beta_q}{\beta} \tag{A.25b}$$

Some typical field distributions of TM modes are shown in Fig. A.3.

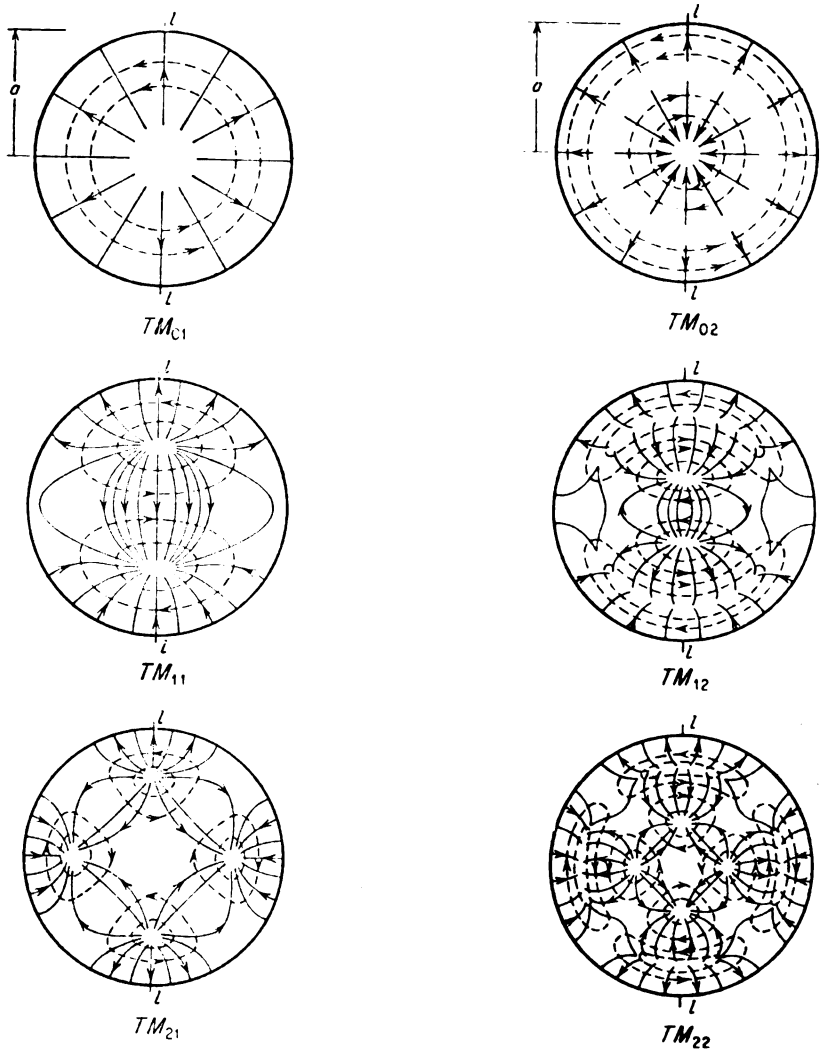

Fig. A. 3. Field configurations in a circular waveguide for TM modes.

REFERENCES

(1) H. W. Ehrenspeck, "The Backfire Antenna, a New Type of Directional Line Source," Proc. IRE, Vol. 48, pp. 109-110, January 1960.

(2) H. W. Ehrenspeck, "The Backfire Antenna: New Results," Proc. IEEE, Vol. 53, pp. 639-641, June 1965.

(3) H. W. Ehrenspeck, "The Short-Backfire Antenna," Proc. IEEE, Vol. 53, pp. 1138-1140, August 1965.

(4) K. M. Chen, D. P. Nyquist and J. L. Lin, "Radiation Fields of the Short-Backfire Antenna," IEEE Trans. Antennas and Propagation, Vol. AP-16, pp. 596-597, September 1968.

(5) F. J. Zucker, "The Backfire Antenna: A Qualitative Approach to Its Design," Proc. IEEE, Vol. 53, pp. 746-747, July 1965.

(6) R. E. Collin, "Foundations for Microwave Engineering," McGraw-Hill Book Co., 1967.

(7) H. Y. Yee and L. B. Felsen, "Ray-Optical Analysis of Electromagnetic Scattering in Waveguides," IEEE Trans. on Microwave Theory and Techniques, Vol. MTT-17, No. 9, pp. 671-683, September 1969.

(8) S. Silver, "Microwave Antenna Theory and Design," Dover Publications, Inc., 1965.

(9) L. A. Wainstein, "Theory of Diffraction and Method of Factorization," Moscow: Izd., Soviet Radio, 1966.

(10) E. A. Wolff, "Antenna Analysis," John Wiley & Son, Inc., 1965.

(11) R. W. P. King, "The Theory of Linear Antennas," Harvard University Press, 1956.

(12) R. F. Harrington, "Matrix Methods for Field Problems," Proc. IEEE, Vol. 55, pp. 136-149, February 1967.

(13) R. W. P. King, "Transmission-Line Theory," Dover Publications, Inc., 1965.